NASA/TM-2006-214282

A Thermodynamically Consistent Damage Model for Advanced Composites

Pere Maimí
Escola Politècnica Superior, Universitat de Girona, Girona, Spain

Pedro P. Camanho
Faculdade de Engenharia, Universidade do Porto, Porto, Portugal

Joan-Andreu Mayugo
Escola Politècnica Superior, Universitat de Girona, Girona, Spain

Carlos G. Dávila
Langley Research Center, Hampton, Virginia

March 2006

The NASA STI Program Office . . . in Profile

Since its founding, NASA has been dedicated to the advancement of aeronautics and space science. The NASA Scientific and Technical Information (STI) Program Office plays a key part in helping NASA maintain this important role.

The NASA STI Program Office is operated by Langley Research Center, the lead center for NASA's scientific and technical information. The NASA STI Program Office provides access to the NASA STI Database, the largest collection of aeronautical and space science STI in the world. The Program Office is also NASA's institutional mechanism for disseminating the results of its research and development activities. These results are published by NASA in the NASA STI Report Series, which includes the following report types:

- TECHNICAL PUBLICATION. Reports of completed research or a major significant phase of research that present the results of NASA programs and include extensive data or theoretical analysis. Includes compilations of significant scientific and technical data and information deemed to be of continuing reference value. NASA counterpart of peer-reviewed formal professional papers, but having less stringent limitations on manuscript length and extent of graphic presentations.

- TECHNICAL MEMORANDUM. Scientific and technical findings that are preliminary or of specialized interest, e.g., quick release reports, working papers, and bibliographies that contain minimal annotation. Does not contain extensive analysis.

- CONTRACTOR REPORT. Scientific and technical findings by NASA-sponsored contractors and grantees.

- CONFERENCE PUBLICATION. Collected papers from scientific and technical conferences, symposia, seminars, or other meetings sponsored or co-sponsored by NASA.

- SPECIAL PUBLICATION. Scientific, technical, or historical information from NASA programs, projects, and missions, often concerned with subjects having substantial public interest.

- TECHNICAL TRANSLATION. English-language translations of foreign scientific and technical material pertinent to NASA's mission.

Specialized services that complement the STI Program Office's diverse offerings include creating custom thesauri, building customized databases, organizing and publishing research results ... even providing videos.

For more information about the NASA STI Program Office, see the following:

- Access the NASA STI Program Home Page at ***http://www.sti.nasa.gov***

- E-mail your question via the Internet to help@sti.nasa.gov

- Fax your question to the NASA STI Help Desk at (301) 621-0134

- Phone the NASA STI Help Desk at (301) 621-0390

- Write to:
  NASA STI Help Desk
  NASA Center for AeroSpace Information
  7121 Standard Drive
  Hanover, MD 21076-1320

NASA/TM-2006-214282

A Thermodynamically Consistent Damage Model for Advanced Composites

Pere Maimí
Escola Politècnica Superior, Universitat de Girona, Girona, Spain

Pedro P. Camanho
Faculdade de Engenharia, Universidade do Porto, Porto, Portugal

Joan-Andreu Mayugo
Escola Politècnica Superior, Universitat de Girona, Girona, Spain

Carlos G. Dávila
Langley Research Center, Hampton, Virginia

National Aeronautics and
Space Administration

Langley Research Center
Hampton, Virginia 23681-2199

March 2006

Available from:

NASA Center for AeroSpace Information (CASI)
7121 Standard Drive
Hanover, MD 21076-1320
(301) 621-0390

National Technical Information Service (NTIS)
5285 Port Royal Road
Springfield, VA 22161-2171
(703) 605-6000

A Thermodynamically Consistent Damage Model for Advanced Composites

P. Maimí [a], P.P. Camanho [b], J.A. Mayugo [a], C.G. Dávila [c]

[a] *AMADE, Escola Politècnica Superior, Universitat de Girona, Girona, Spain*

[b] *DEMEGI, Faculdade de Engenharia, Universidade do Porto, Rua Dr. Roberto Frias, 4200-465 Porto, Portugal*

[c] *NASA Langley Research Center, Hampton, VA 23681,U.S.A.*

Abstract

A continuum damage model for the prediction of damage onset and structural collapse of structures manufactured in fiber-reinforced plastic laminates is proposed. The principal damage mechanisms occurring in the longitudinal and transverse directions of a ply are represented by a damage tensor that is fixed in space. Crack closure under load reversal effects are taken into account using damage variables established as a function of the sign of the components of the stress tensor. Damage activation functions based on the LaRC04 failure criteria are used to predict the different damage mechanisms occurring at the ply level. The constitutive damage model is implemented in a finite element code. The objectivity of the numerical model is assured by regularizing the dissipated energy at a material point using Bažant's Crack Band Model. To verify the accuracy of the approach, analyses of coupon specimens were performed, and the numerical predictions were compared with experimental data.

Key words: Fracture Mechanics, Continuum Damage Mechanics, Composite Materials.

1 INTRODUCTION

The methodology for designing high-performance structures of composite materials is still evolving. The complexity of the response of composite materials and the difficulty in predicting structural modes of failure result in the need for a well-planned test program. The recommended practice to mitigate the technological risks associated with such materials is to substantiate the performance and durability of the design in a sequence of steps known as the

Building Block Approach (BBA)[1]. The BBA ensures that cost and performance objectives are met by testing greater numbers of smaller less expensive specimens, assessing technology risks early in the program, and building on the knowledge acquired at a given level of structural complexity before progressing to a level of more complexity.

Achieving substantiation of structural performance by testing alone can be prohibitively expensive because of the number of specimens and components required to characterize all loading conditions. BBA programs can achieve significant cost reductions by seeking a synergy between testing and analysis. The more the development relies on analysis, the less expensive it becomes.

The use of advanced analytical or numerical models for the prediction of the mechanical behavior of composite structures can replace some of the mechanical tests and can significantly reduce the cost of designing with composites while providing to the engineers the information necessary to achieve an optimized design.

Strength-based failure criteria are commonly used to predict failure in composite materials. A large number of continuum-based criteria have been derived to relate stresses and experimental measures of material strength to the onset of failure [2]-[4]. Failure criteria predict the onset of the different damage mechanisms occurring in composites and, depending on the material, the geometry and the loading conditions, may also predict final structural collapse.

For composite structures that can accumulate damage before structural collapse, the use of failure criteria is not sufficient to predict ultimate failure. Simplified models, such as the ply discount method, can be used to predict ultimate failure, but they cannot represent with satisfactory accuracy the quasi-brittle failure of laminates that results from the accumulation of several damage mechanisms.

The study of the non-linear response of quasi-brittle materials due to the accumulation of damage is important because the rate and direction of damage propagation defines the damage tolerance of a structure and its eventual collapse. To model the phenomena of damage propagation, non-linear constitutive models defined in the context of the mechanics of continuum mediums have been developed and implemented in finite elements codes in recent years. The formalism of the thermodynamics of irreversible processes is a rigorous framework from which the constitutive models can be developed.

The simplest way to describe damage is using a single scalar damage variable as proposed by Kachanov [5]. Damage can be interpreted as the creation of microcavities, and the damage variables as a measure of the effective surface density of the microdefects. Such a mechanical interpretation of damage assumes that the loads are resisted only by the undamaged ligaments in the

material. The stresses ($\tilde{\sigma}$) in the ligaments, referred to as effective stresses, continue to increase until all ligaments are severed and the material has failed.

The tensorial representation of damage is a formal and general procedure to represent the directionality of micro-cracks, which can take any direction in a medium depending on the load history, geometry, boundary conditions, and material properties. After Kachanov's pioneering work, several damage models have been developed that describe damage as a second order tensor [6]-[9] or as a fourth order tensor [10]-[12]. Second order tensors describe an initially isotropic material as an orthotropic one when damage evolves, whereas fourth order tensor models can remove all material symmetries and provide a more general procedure to simulate damage [13].

The application of continuum damage models in orthotropic or transversely isotropic materials, such as fiber-reinforced plastics (FRP), results in additional difficulties. The nature and morphology of a material induces some preferred directions for crack growth, i.e., crack orientations are not only induced by the loads, geometry and boundary conditions, but also by the morphology of the material. The interface between fiber and matrix is weaker than the surrounding material and interfacial debonding is normally the first damage mechanism to occur. Furthermore, residual thermal stresses occur in the composite plies due to different coefficients of thermal expansion of the fiber and matrix (micromechanical residual thermal stresses) and due to the different coefficients of thermal expansion in the longitudinal (fiber) and transverse (matrix) directions (macromechanical residual thermal stresses).

Multiscale models and mesomodeling are two approaches used to evaluate the elastic and inelastic response of a material. Using homogenization laws, multiscale models define relations between a mesoscale, normally the scale of the finite elements, where material is considered homogeneous, and the microscale the scale of constituents, fiber and matrix. The constitutive models are defined at the microscale, and the strain and stress fields at the microscale and the mesoscale are related via transformation field tensors [14]-[18], or solved using finite elements [18],[19]. To reduce the amount of computations that need to be performed, periodicity of the material is invoked.

Mesomodeling is an alternative way to define damage models for composite materials that is more appropriate for large scale computations. Mesomodels treat the composite lamina [20]-[24] or sub-laminate [25] as a homogeneous material. When diffuse damage localizes in a narrow band and becomes a macro-crack, the response is dominated by the crack tip and its ability to dissipate energy. On the other hand, the material morphology, which is the main basis of homogenization techniques, loses importance due to the loss of periodicity. Therefore, in structures exhibiting stable crack propagation, i.e., when the macrocrack length does not increase under constant load, mesomodeling is more appropriate to predict the structural collapse than multiscale models.

The main objective of the present paper is to develop a continuum damage model able to represent the quasi-brittle fracture of laminated composite structures, from damage onset up to final structural collapse.

The majority of the material properties required by the present model can be measured using standard test methods. Most of the material properties that are required can be obtained from ply-based test methods. The use of ply properties, rather than laminate properties, is an advantage because it avoids the need to test laminates every time the lay-up or stacking sequence is modified.

The proposed constitutive model accounts for crack closure under load reversal effects, an important phenomenon in cases where a composite structure is subjected to multiaxial loading.

One important issue regarding the numerical modeling of damage is that the convergence of the solution through successive mesh refinement must be ensured. The objectivity of the numerical model is ensured by adjusting the energy dissipated by each damage mechanism using a characteristic element length. The constitutive model proposed herein can be integrated explicitly, making it computationally efficient and, therefore, suitable to be used in large scale computations.

This paper is organized as follows: a brief description of the damage mechanisms occurring in laminated composites is presented. Based on the mechanisms of damage identified, a new constitutive damage model is proposed. The constitutive model relates the damage mechanisms with a set of internal variables. The constitutive model is implemented in a non-linear finite element code, and it is adjusted using a procedure based on Bažant's Crack Band Model [26] that ensures the correct computation of the energy dissipated by each damage mechanism. The accuracy of the model is assessed by comparing the predictions with experimental data for an open-hole tension carbon-fiber specimen.

2 MECHANISMS OF DAMAGE AND FRACTURE IN LAMINATED COMPOSITES

2.1 Longitudinal failure

In fiber-reinforced composites, the largest portion of the loads is resisted by the fibers. When these fail under either tension or compression, the internal loads must redistribute to other areas of the structure, and may cause a structural collapse.

In composites with high fiber volume fraction and those where the strain to failure of the resin matrix is higher than the one of the reinforcing fiber, such as carbon-epoxy composites, longitudinal failures start by isolated fibre fractures in weak zones. The localized fractures increase the normal and interfacial shear stresses in the adjoining fibers, and the local stress concentrations promote matrix cracking, fibre matrix debonding and, for ductile matrices, conical shear failures [27]. When increasing the load further, additional fibre fractures occur, leading to final collapse.

Failure under longitudinal tensile loading occurs in both constituents, and fracture occurs along a plane that is parallel to the fibers and the thickness direction (Figure 1). A simple non-interacting failure criterion based on maximum stress or maximum strain along the longitudinal direction can usually provide an accurate measure of longitudinal tensile failure [3].

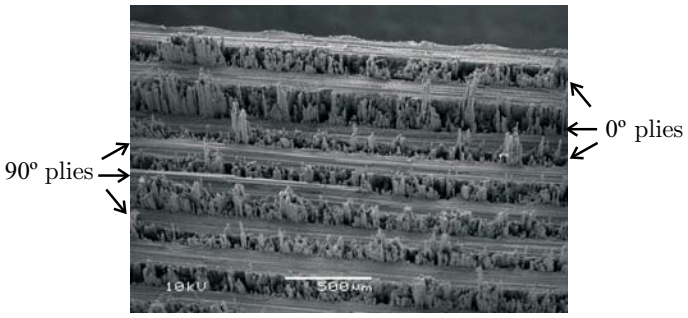

Fig. 1. Longitudinal failure in 0° plies [28].

Compressive failure of aligned fiber composites occurs from the collapse of the fibers as a result of shear kinking and damage of the supporting matrix [29],[30]. A kink band in a carbon-epoxy laminate resulting from compressive longitudinal stresses is shown in Figure 2.

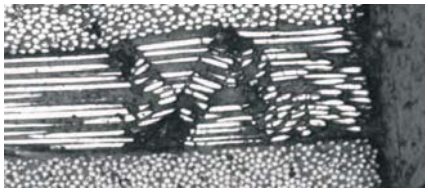

Fig. 2. Kink band in a 0° ply [31].

Argon [32] was the first to analyze the kinking phenomenon, based on the assumption of a local initial fiber misalignment. Fiber misalignment causes shear stresses between fibers that rotate the fibers, which in turn increase the shear stress and leads to instability.

Recently, the calculation of the critical kinking stress has been significantly improved with a more complete understanding of the geometry of the kink band as well as the incorporation of friction and material nonlinearity in the analysis models [28],[33].

2.2 Transverse failure

Failure in the transverse direction encompasses both matrix cracking and fiber-matrix debonding. Under the presence of transverse tensile stresses and in-plane shear stresses, the combined effect of small defects present in a ply such as small fiber-resin debonds, resin-rich regions, and resin voids, trigger a transverse crack that extends through the thickness of the ply (Figure 3). The transverse cracks are formed without disturbing the fibers: they occur at the fiber-resin interface and in the resin.

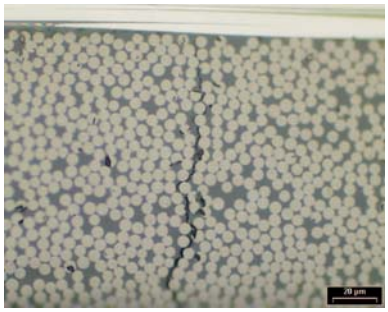

Fig. 3. Transverse matrix crack in a 90° ply.

A fundamental issue that needs to be considered is the effect of ply thickness on the ply strength, usually called the 'in-situ effect'. As shown in Parvizi [34] and Chang's [35] experiments, the constraints imposed by the neighboring plies of different fiber orientations cause an apparent increase in the tensile

and shear strengths of a ply compared to those of an unconstrained ply. The scale effect for the in-plane shear strength is represented in Figure 4 , where it is apparent that the strength of a ply is a function of the number of 90° plies stacked together using the model proposed by Camanho et al. [36].

The in-situ effect is a deterministic size effect that can be represented using fracture mechanics models of plies containing defects [3],[37].

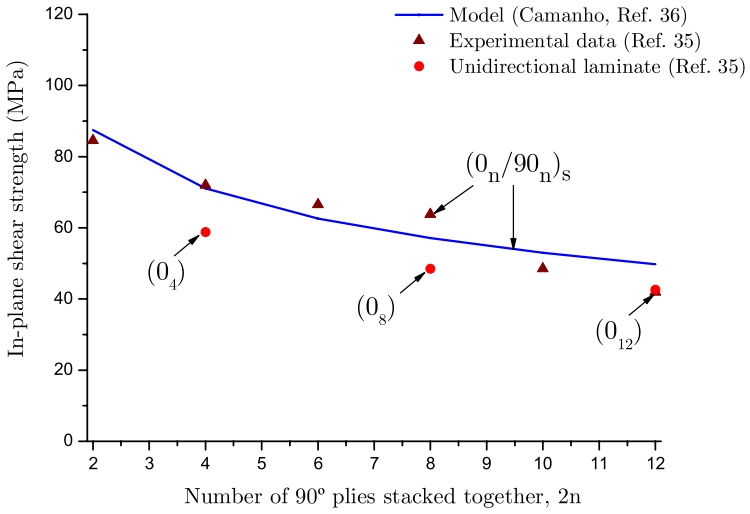

Fig. 4. In-situ shear strength of T300/1034-C CFRP.

Experimental results have shown that moderate values of transverse compression have a beneficial effect on the strength of a ply. This effect can be observed in the experimental results obtained by Swanson [38],[39] shown in Figure 5. The failure envelope calculated using the LaRC04 failure criterion [4] is also shown in Figure 5.

When the in-plane shear stress is large compared to the transverse compressive stress, the fracture plane is perpendicular to the midplane of the ply. This mode of failure is referred to as Mode A in Figure 5. However, increasing the compressive transverse stress causes a change in the angle of the fracture plane, as shown in Figure 6. This mode of failure is referred to as Mode B in Figure 5. Normally, for carbon-epoxy and glass-epoxy composites loaded in pure transverse compression, the fracture plane is at an angle (fracture angle, α_0) of $53° \pm 3°$ with respect to the thickness direction [40]. Therefore, matrix cracking does not occur in the plane of the maximum transverse shear stress (45°).

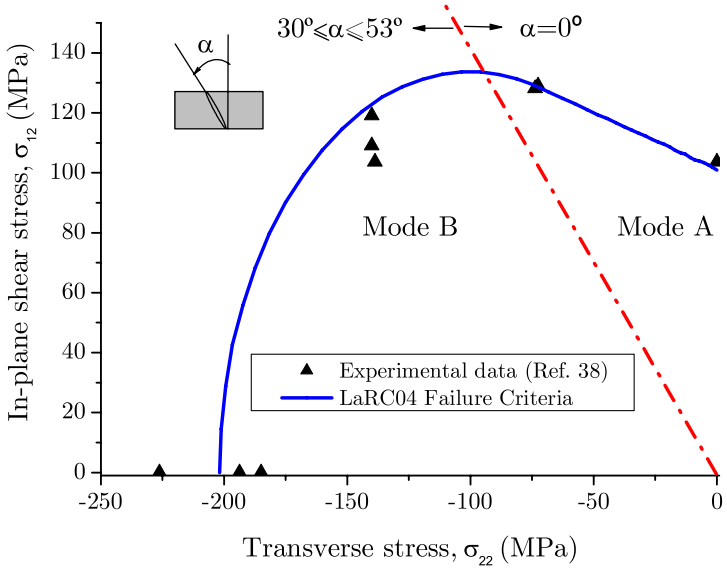

Fig. 5. Strength as a function of transverse compression and in-plane shear.

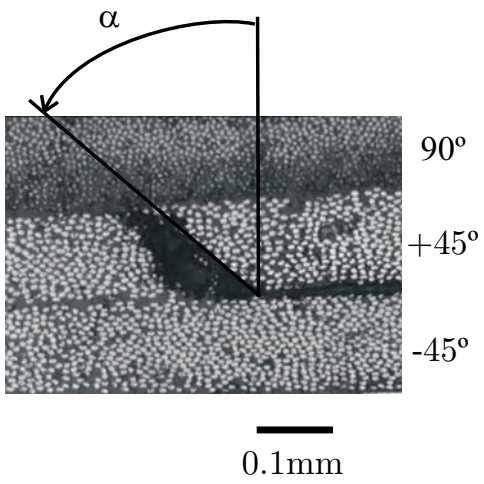

Fig. 6. Matrix crack in a 45° ply created by in-plane compressive transverse stress [31].

2.3 Delamination

Delamination is a common damage mechanism in multidirectional laminated composites due to their weakness in the thickness direction. The three dimensional stress states that occur near geometric discontinuities such as ply drop-offs, stiffener terminations, flanges, bonded and bolted joints, and access holes promote delamination initiation. Delamination causes a reduction of the bending stiffness of a composite structure and, when compressive loads are present, promotes local buckling.

Delamination models [41]-[44] always represent a discrete crack separating elements as do, for concrete, the pioneering work of Dudgale-Barenblatt [45],[46]. The purpose of present work is to propose a Continuum Damage Mechanics (CDM) model for the calculation of the initiation and propagation of intralaminar damage. Consequently, delamination damage is not considered here.

3 CONSTITUTIVE DAMAGE MODEL

The thermodynamics of irreversible processes is a general framework that can be used to formulate constitutive equations. It is a logical framework for incorporating observations and experimental results and a set of rules for avoiding incompatibilities. In this section, we present a constitutive damage model for laminated composites that has its foundation in irreversible thermodynamics, and that uses the LaRC04 criteria as damage activation functions.

3.1 Complementary free energy and damage operator

To establish a constitutive law, it is necessary to define a scalar function corresponding to the complementary free energy density in the material. This function must be positive definite, and it must be zero at the origin with respect to the free variables (the stresses) [47]. The proposed definition for the complementary free energy density is:

$$G = \frac{\sigma_{11}^2}{2\left(1-d_1\right)E_1} + \frac{\sigma_{22}^2}{2\left(1-d_2\right)E_2} - \frac{\nu_{12}}{E_1}\sigma_{11}\sigma_{22} + \frac{\sigma_{12}^2}{2\left(1-d_6\right)G_{12}} + \\ + \left(\alpha_{11}\sigma_{11} + \alpha_{22}\sigma_{22}\right)\Delta T + \left(\beta_{11}\sigma_{11} + \beta_{22}\sigma_{22}\right)\Delta M \qquad (1)$$

where E_1, E_2, ν_{12} and G_{12} are the in-plane elastic orthotropic properties of a unidirectional lamina. The subscript 1 denotes the longitudinal (fiber) di-

rection, and 2 denotes the transverse (matrix) direction. The damage variable d_1 is associated with longitudinal (fiber) failure, whereas d_2 is the damage variable associated with transverse matrix cracking and d_6 is a damage variable influenced by longitudinal and transverse cracks. α_{11} and α_{22} are the coefficients of thermal expansion in the longitudinal and transverse directions, respectively. β_{11} and β_{22} are the coefficients of hygroscopic expansion in the longitudinal and transverse directions, respectively. ΔT and ΔM are the differences of temperature and moisture content with respect to the corresponding reference values.

The stress tensor σ corresponds to the average stress tensor over a representative volume that is assumed to be much larger than the diameter of a fiber.

To ensure the thermodynamically irreversibility of the damage process, the rate of change of the complementary free energy $\dot{G}$ minus the externally supplied work to the solid $\dot{\sigma} : \varepsilon$ at constant strains, must not be negative:

$$\dot{G} - \dot{\sigma} : \varepsilon \geq 0 \tag{2}$$

This inequality corresponds to the positiveness of the dissipated energy and has to be fulfilled by any constitutive model [47]. Expanding the inequality in terms of the stress tensor and damage variables gives:

$$\left(\frac{\partial G}{\partial \sigma} - \varepsilon \right) : \dot{\sigma} + \frac{\partial G}{\partial d} \cdot \dot{d} \geq 0 \tag{3}$$

Since the stresses are variables that can vary freely, the expression in the parenthesis must be equal to zero to ensure positive dissipation of mechanical energy. Therefore, the strain tensor is equal to the derivative of the complementary free energy density with respect to the stress tensor:

$$\varepsilon = \frac{\partial G}{\partial \sigma} = \mathbf{H} : \sigma + \alpha \Delta T + \beta \Delta M \tag{4}$$

The lamina compliance tensor can be represented in Voigt notation as:

$$\mathbf{H} = \frac{\partial^2 G}{\partial \sigma^2} = \begin{bmatrix} \dfrac{1}{(1-d_1)\,E_1} & -\dfrac{\nu_{21}}{E_2} & 0 \\ -\dfrac{\nu_{12}}{E_1} & \dfrac{1}{(1-d_2)\,E_2} & 0 \\ 0 & 0 & \dfrac{1}{(1-d_6)\,G_{12}} \end{bmatrix} \tag{5}$$

The closure of transverse cracks under load reversal, also known as the unilateral effect, is taken into account by defining four damage variables associated with longitudinal and transverse damage. To determine the active damage variables, it is necessary to define the longitudinal and transverse damage modes as follows:

$$\begin{aligned} d_1 &= d_{1+}\frac{\langle\sigma_{11}\rangle}{|\sigma_{11}|} + d_{1-}\frac{\langle-\sigma_{11}\rangle}{|\sigma_{11}|} \\ d_2 &= d_{2+}\frac{\langle\sigma_{22}\rangle}{|\sigma_{22}|} + d_{2-}\frac{\langle-\sigma_{22}\rangle}{|\sigma_{22}|} \end{aligned} \tag{6}$$

where $\langle x\rangle$ is the McCauley operator defined as $\langle x\rangle := (x + |x|)/2$.

The present model tracks damage caused by tension loads (d_+) separately from damage caused by compression loads (d_-). Depending on the sign of the corresponding normal stress, a damage mode can be either active or passive.

The model also assumes that the shear damage variable, d_6, is not affected by the closure effect. Shear damage is caused mainly by transverse cracks and these do not close under shear stresses (σ_{12}). Transverse cracks are influenced by transverse stresses (σ_{22}) producing the closure of cracks and a friction retention whereas longitudinal cracks produce the same effect under longitudinal stresses (σ_{11}) [48]. The effect of friction is neglected in the present model.

3.2 Damage activation functions

The determination of the domain of elastic response under complex stress states is an essential component of an accurate damage model. Based on the previously described mechanisms of crack generation in advanced composites, a strain space is considered where the material is linear elastic. In the present model, it is assumed that the elastic domain is enclosed by four surfaces, each of them accounting for one damage mechanism: longitudinal and transverse fracture under tension and compression. Those surfaces are formulated by the damage activation functions based on the LaRC03 and LaRC04 failure criteria. The LaRC03-04 failure criteria have been shown to represent accurately the physical process of damage onset in laminated composites. The LaRC04 criteria represent an evolution of the LaRC03 criteria: some criteria such as the one for fiber kinking, are more accurate in LaRC04. However, the improvement in accuracy is associated with a significant increase in the computational effort. The present damage model uses a combination of both sets of criteria to achieve a compromise between accuracy and computational efficiency. The full details of the derivation and validation of the LaRC04 failure criteria are presented in references [3],[4].

The four damage activation functions, F_N, associated with damage in the longitudinal ($N = 1+, 1-$) and transverse ($N = 2+, 2-$) directions, are defined as:

$$\begin{aligned} F_{1+} = \phi_{1+} - r_{1+} \leq 0 \ ; \ F_{1-} = \phi_{1-} - r_{1-} \leq 0 \\ F_{2+} = \phi_{2+} - r_{2+} \leq 0 \ ; \ F_{2-} = \phi_{2-} - r_{2-} \leq 0 \end{aligned} \tag{7}$$

where the loading functions ϕ_N ($N = 1+, 1-, 2+, 2-$) depend on the strain tensor and material constants (elastic and strength properties). The elastic domain thresholds r_N ($N = 1+, 1-, 2+, 2-$) take an initial value of 1 when the material is undamaged, and they increase with damage. The elastic domain thresholds are internal variables of the constitutive model, and are related to the damage variables d_M ($M = 1+, 1-, 2+, 2-, 6$) by the damage evolution laws. The elastic domain threshold defines the level of elastic strains that can be attained before the accumulation of additional damage.

3.2.1 Longitudinal tensile fracture

The LaRC04 criterion for fiber tension failure is a non-interacting maximum allowable strain criterion defined as:

$$\phi_{1+} = \frac{E_1}{X_T}\varepsilon_{11} = \frac{\tilde{\sigma}_{11} - \nu_{12}\tilde{\sigma}_{22}}{X_T} \tag{8}$$

where the effective stress tensor $\tilde{\sigma}$ is computed as $\tilde{\sigma} = \mathbf{H_0}^{-1} : \varepsilon$. $\mathbf{H_0}$ is the undamaged compliance tensor obtained from equation (5) using $d_1 = d_2 = d_6 = 0$.

3.2.2 Longitudinal compressive fracture

The LaRC03 failure criterion for longitudinal compressive fracture postulates that a kink band is triggered by the onset of damage in the supporting matrix. Under this circumstance, the fibres lose lateral support and fail under the effect of longitudinal compressive stresses. The initial fiber misalignment and the rotation of the fibers as a function of the applied stress state are the parameters used in the damage activation function.

The damage activation function used to predict damage under longitudinal compression ($\tilde{\sigma}_{11} < 0$) and in-plane shear (fiber kinking) is established as a

function of the components of the stress tensor $\tilde{\sigma}^{(m)}$ in a coordinate system (m) representing the fiber misalignment:

$$\phi_{1-} = \frac{\left\langle |\tilde{\sigma}_{12}^{m}| + \eta^{L}\tilde{\sigma}_{22}^{m} \right\rangle}{S_L} \tag{9}$$

where the longitudinal friction coefficient can be approximated as [3]:

$$\eta^{L} \approx -\frac{S_L \cos(2\alpha_0)}{Y_C \cos^2 \alpha_0} \tag{10}$$

The components of the effective stress tensor in the coordinate system associated with the rotation of the fibers are calculated as:

$$\begin{aligned} \tilde{\sigma}_{22}^{m} &= \tilde{\sigma}_{11} \sin^2 \varphi^{C} + \tilde{\sigma}_{22} \cos^2 \varphi^{C} - 2\,|\tilde{\sigma}_{12}| \sin \varphi^{C} \cos \varphi^{C} \\ \tilde{\sigma}_{12}^{m} &= (\tilde{\sigma}_{22} - \tilde{\sigma}_{11}) \sin \varphi^{C} \cos \varphi^{C} + |\tilde{\sigma}_{12}| \left(\cos^2 \varphi^{C} - \sin^2 \varphi^{C} \right) \end{aligned} \tag{11}$$

where the absolute value of the shear stress is taken because the misalignment angle can be positive or negative.

The misalignment angle (φ^{C}) is determined using standard shear and longitudinal compression strengths, S_L and X_C [3]:

$$\varphi^{C} = \arctan\left(\frac{1 - \sqrt{1 - 4\left(\frac{S_L}{X_C} + \eta^{L}\right)\frac{S_L}{X_C}}}{2\left(\frac{S_L}{X_C} + \eta^{L}\right)} \right) \tag{12}$$

It should be noted that the LaRC03 failure criterion, derived to predict the onset of damage in laminated composites, calculates the misalignment angle as a function of the applied stress. The LaRC03 failure criterion is modified here assuming a constant misalignment angle, corresponding to the rotation of the fibres at failure under pure longitudinal compression. This modification of LaRC03 failure criterion assures that ϕ_{1-} is a monotonic increasing function under any state of proportional loading.

It should be pointed out that two criteria are used in LaRC03 for fiber kinking: Equation (9) for $\tilde{\sigma}_{22}^{m} \leq 0$ and a second equation for $\tilde{\sigma}_{22}^{m} \geq 0$. However, the omission of the second equation results in a minor loss of accuracy because the equation is the same as equation (13.a) (below) with the stresses transformed into the misaligned coordinate frame.

3.2.3 Transverse fracture perpendicular to the laminate mid-plane ($\alpha_0 = 0°$)

Transverse matrix cracks perpendicular to the mid-plane of the ply, i.e. with $\alpha_0 = 0°$ (Figures 6 and 5), are created by a combination of in-plane shear stresses and transverse tensile stresses, or in-plane shear stresses and small transverse compressive stresses. These conditions are represented by the following LaRC04 failure criterion:

$$\phi_{2+} = \begin{cases} \sqrt{(1-g)\,\dfrac{\tilde{\sigma}_{22}}{Y_T} + g\left(\dfrac{\tilde{\sigma}_{22}}{Y_T}\right)^2 + \left(\dfrac{\tilde{\sigma}_{12}}{S_L}\right)^2} & \text{if } \tilde{\sigma}_{22} \geq 0 \\ \dfrac{1}{S_L}\left\langle |\tilde{\sigma}_{12}| + \eta^L \tilde{\sigma}_{22} \right\rangle & \text{if } \tilde{\sigma}_{22} < 0 \end{cases} \tag{13}$$

where g is the fracture toughness ratio defined as: $g = \frac{\mathrm{G_{Ic}}}{\mathrm{G_{IIc}}}$.

3.2.4 Transverse fracture with $\alpha_0 = 53°$

The LaRC04 matrix failure criterion for transverse compressive stresses consists of a quadratic interaction between the effective shear stresses acting on the fracture plane:

$$\phi_{2-} = \sqrt{\left(\frac{\tilde{\tau}^T_{\text{eff}}}{S_T}\right)^2 + \left(\frac{\tilde{\tau}^L_{\text{eff}}}{S_L}\right)^2} \text{ if } \tilde{\sigma}_{22} < 0 \tag{14}$$

where the effective stresses $\tilde{\tau}^T_{\text{eff}}$ and $\tilde{\tau}^L_{\text{eff}}$ are computed as [4]:

$$\begin{aligned} \tilde{\tau}^T_{\text{eff}} &= \left\langle -\tilde{\sigma}_{22}\cos(\alpha_0)\left(\sin(\alpha_0) - \eta^T \cos(\alpha_0)\cos(\theta)\right)\right\rangle \\ \tilde{\tau}^L_{\text{eff}} &= \left\langle \cos(\alpha_0)\left(|\tilde{\sigma}_{12}| + \eta^L \tilde{\sigma}_{22}\cos(\alpha_0)\sin(\theta)\right)\right\rangle \end{aligned} \tag{15}$$

The sliding angle θ is calculated as [4]:

$$\theta = \arctan\left(\frac{-|\tilde{\sigma}_{12}|}{\tilde{\sigma}_{22}\sin(\alpha_0)}\right) \tag{16}$$

The transverse shear strength and transverse friction coefficient can be approximated as:

$$\begin{aligned} S_T &= Y_C \cos(\alpha_0)\left[\sin(\alpha_0) + \tfrac{\cos(\alpha_0)}{\tan(2\alpha_0)}\right] \\ \eta^T &= \tfrac{-1}{\tan(2\alpha_0)} \end{aligned} \tag{17}$$

The fracture angle α_0 is approximately 53° in uniaxial compression. With increasing amounts of in-plane shear, the fracture angle diminishes up to about 40° (Mode B in figure 5) and then abruptly switches to 0^0 (Mode A in figure 5). To find the correct angle of fracture, a maximization of the LaRC03-04 failure criteria as a function of α should be performed. However, in order to improve the computational efficiency of the present model, it is assumed that the fracture angle can only take one of two discrete values: 0° or 53°.

The elastic domain in the $\tilde{\sigma}_{11}$, $\tilde{\sigma}_{22}$, $\tilde{\sigma}_{12}$ space represented by the LaRC04 failure criteria is shown in Figure 7.

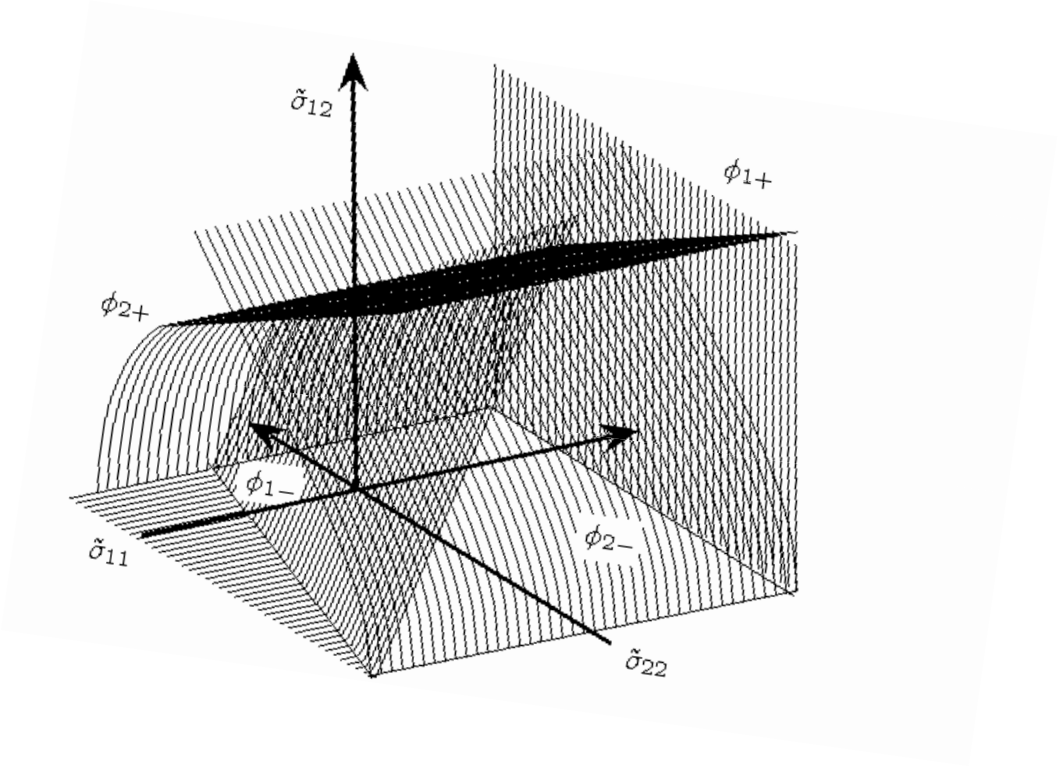

Fig. 7. Elastic domain in the $\tilde{\sigma}_{11}$, $\tilde{\sigma}_{22}$, $\tilde{\sigma}_{12}$ space.

3.3 Dissipation

The rate of energy dissipation per unit volume resulting from the evolution of damage is given by:

$$\Xi = \frac{\partial G}{\partial d_1}\dot{d}_1 + \frac{\partial G}{\partial d_2}\dot{d}_2 + \frac{\partial G}{\partial d_6}\dot{d}_6 = Y_1\dot{d}_1 + Y_2\dot{d}_2 + Y_6\dot{d}_6 \geq 0 \tag{18}$$

The form of the complementary free energy defined in equation (1) assures that the thermodynamic forces (Y_M) conjugated to their respective damage variables (d_M) are always positive:

$$
\begin{aligned}
Y_1 &= \frac{\partial G}{\partial d_1} = \frac{\sigma_{11}^2}{2(1-d_1)^2 E_1} \geq 0 \\
Y_2 &= \frac{\partial G}{\partial d_2} = \frac{\sigma_{22}^2}{2(1-d_2)^2 E_2} \geq 0 \\
Y_6 &= \frac{\partial G}{\partial d_6} = \frac{\sigma_{12}^2}{2(1-d_6)^2 G_{12}} \geq 0
\end{aligned}
\tag{19}
$$

Therefore, the condition of positive evolution of damage variables ($\dot{d}_M \geq 0$) is a sufficient condition for the fulfillment of the second law of thermodynamics.

It is important to note that the proposed model does not generate spurious energy dissipation, i.e., the loss or gain of mechanical energy, under crack closure or opening. At load reversal, the time derivative of the damage variable is non-zero ($\dot{d}_M \neq 0$). Considering equation (18), the thermodynamical forces, Y_M, associated with the damage variables, d_M, must be zero to avoid spurious energy dissipation at load reversal [49]. This condition is trivially satisfied in the present model (equation (19)).

Damage evolution without energy dissipation is physically inadmissible. Therefore, it is necessary to avoid damage evolution when the corresponding conjugated thermodynamic force is zero. Consider the load history represented in Figure 8: the material is loaded in transverse tension and shear to t_1 and then loaded to t_2. At time t_2, the damage variable d_2 evolves because the corresponding damage activation function is activated. However, the corresponding thermodynamic force is zero ($\sigma_{22} = 0$, $Y_2 = 0$).

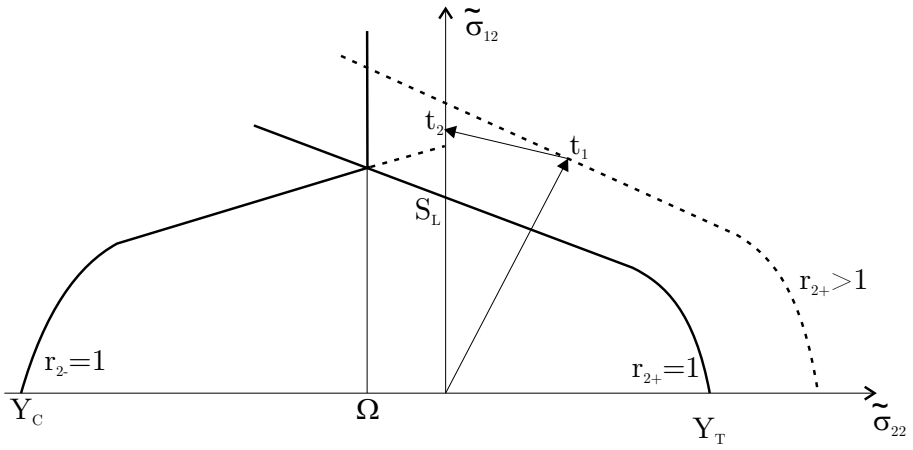

Fig. 8. Evolution of elastic domain in the $\tilde{\sigma}_{22} - \tilde{\sigma}_{12}$ space.

This non-physical response is avoided by modifying the longitudinal and transverse damage activation functions. The transverse damage activation function is modified using the following equation:

$$\phi_{2-} = \min \left\{ \sqrt{\left(\frac{\tilde{\tau}_{\text{eff}}^{T}}{S_T}\right)^2 + \left(\frac{\tilde{\tau}_{\text{eff}}^{L}}{S_L}\right)^2}, \frac{\tilde{\sigma}_{22}}{\Omega} \right\} \tag{20}$$

where the constant Ω is equal to $\tilde{\sigma}_{22}$ when ϕ_{2-}=ϕ_{2+} (Figure 8).

The longitudinal damage activation function is modified by taking into account that under shear dominated loads, matrix cracking is the first form of damage to occur. After matrix cracking, the transverse and shear stresses are zero and the fiber misalignment angle φ tends to $\pi/4$. Under these circumstances, the kink band criteria, equation (9), reads:

$$\phi_{1-} = \min \left\{ \frac{\left\langle |\tilde{\sigma}_{12}^{m}| + \eta^{L} \tilde{\sigma}_{22}^{m} \right\rangle}{S_L}, \frac{\eta^{L} - 1}{2S_L} \tilde{\sigma}_{11} \right\} \tag{21}$$

3.4 Damage evolution

The evolution of the threshold values r_N is mathematically expressed by the *Kuhn-Tucker conditions*:

$$\dot{r}_N \geq 0 \; ; \; F_N \leq 0 \; ; \; \dot{r}_N F_N = 0 \tag{22}$$

Neglecting viscous effects, the damage activation functions, equations (7), always have to be non-positive. While the damage activation function F_N is negative, the material response is elastic. When the strain state activates a criterion, $F_N = 0$, it is necessary to evaluate the gradient $\dot{\phi}_N$. If the gradient is not positive, the state is one of unloading or neutral loading. If the gradient $\dot{\phi}_N$ is positive, there is damage evolution, and the *consistency condition* has to be satisfied:

$$\dot{F}_N = \dot{\phi}_N - \dot{r}_N = 0 \tag{23}$$

Two important characteristics of the model proposed here are that the threshold values are a function of the damage variables, and that the loading functions depend on the strain tensor. Under these conditions, it is possible to explicitly integrate the constitutive model [11],[12].

In the definition of the constitutive model, it is necessary to represent the relation between active and inactive elastic domains. The evolution of an active elastic domain is defined by the consistency condition, i.e., it is defined with

respect to the corresponding damage activation function. However, it is also necessary to specify how the inactive elastic domain evolves if other damage modes are active. It is assumed that the longitudinal and transverse domains are not coupled. On the other hand, compression damage is coupled with tension damage, as explained in the next section.

3.4.1 Transverse loading

As previously described, transverse damage in the form of matrix cracks can have different orientations as a result of tension, shear, or compression-dominated loads. Under load reversal, transverse cracks, which are perpendicular to the ply mid-plane, do not affect the compression response: elastic domain and the compressive damage variable (d_{2-}) are unaffected by r_{2+}.

On the other hand, matrix cracks at a fracture angle $\alpha_0 = 53°$ caused by high compressive transverse stresses have the same effect as cracks perpendicular to the mid-plane ($\alpha = 0°$) when the load is reversed from compression to tension. Therefore, the evolution of the transverse tensile elastic domain threshold (r_{2+}) is governed by both damage mechanisms.

Based on the above considerations, the evolution of the elastic domain in the transverse direction can be represented by the following equations:

$$\text{Tension loading:} \qquad \dot{r}_{2+} = \dot{\phi}_{2+} \text{ and } \dot{r}_{2-} = 0$$

$$\text{Compression loading:} \quad \dot{r}_{2-} = \dot{\phi}_{2-} \text{ and } \dot{r}_{2+} = \begin{cases} \dot{\phi}_{2-} & \text{if } r_{2+} \leq r_{2-} \\ 0 & \text{if } r_{2+} > r_{2-} \end{cases}$$

The integration of the previous expressions results in:

$$\begin{aligned} r_{2+} &= \max\left\{1, \max_{s=0,t}\left\{\phi^s_{2-}\right\}, \max_{s=0,t}\left\{\phi^s_{2+}\right\}\right\} \\ r_{2-} &= \max\left\{1, \max_{s=0,t}\left\{\phi^s_{2-}\right\}\right\} \end{aligned} \tag{24}$$

3.4.2 Longitudinal loading

Under longitudinal tensile stresses, the fracture plane is perpendicular to the fiber direction. When reversing the load, the cracks close and can still transfer load. However, the broken and misaligned fibers do not carry any additional

load. Therefore, the compressive stiffness is influenced by longitudinal damage. However, the elastic domain is assumed to remain unchanged.

Under longitudinal compression, damaged material consisting of broken fibers and matrix cracks forms a kink band, and there is not a unique orientation for the damage planes. When the loads are reversed, the cracks generated in compression open and the elastic domain threshold increases.

Therefore, the evolution of damage thresholds for longitudinal damage are defined as:

$$\begin{aligned} &\text{Tension loading:} && \dot{r}_{1+} = \dot{\phi}_{1+} \text{ and } \dot{r}_{1-} = 0 \\ &\text{Compression loading:} && \dot{r}_{1-} = \dot{\phi}_{1-} \text{ and } \dot{r}_{1+} = \begin{cases} \dot{\phi}_{1-} & \text{if } r_{1+} \leq r_{1-} \\ 0 & \text{if } r_{1+} > r_{1-} \end{cases} \end{aligned} \tag{25}$$

The integration of the previous expressions results in:

$$\begin{aligned} r_{1+} &= \max\left\{1, \max_{s=0,t}\left\{\phi_{1+}^{s}\right\}, \max_{s=0,t}\left\{\phi_{1-}^{s}\right\}\right\} \\ r_{1-} &= \max\left\{1, \max_{s=0,t}\left\{\phi_{1-}^{s}\right\}\right\} \end{aligned} \tag{26}$$

3.5 Damage evolution laws

The internal variables r_N define the threshold of the elastic domains, and are related to the damage state of each lamina, i.e., the damage variables depend on the values of the internal variables. In order to fully define the constitutive model, it is necessary to define the relation between the internal variables and the damage variables.

When material is undamaged the internal variables r_N take the initial value of 1, and $d_N(r_N = 1) = 0$. Equations (24) and (26) define the evolution of the internal variables assuring that $\dot{r}_N \geq 0$. As shown in equations (18) and (19), the condition for positive dissipation is satisfied if $\dot{d}_N \geq 0$. The condition for positive dissipation is automatically fulfilled if the damage evolution law satisfies the condition $\partial d_N / \partial r_N \geq 0$. When the material is completely damaged, a fracture plane is created, the strains are localized in a plane in which $r_N \to \infty$ and the related components of the stiffness tensor are zero, $d_N(r_N \to \infty) = 1$.

Matrix cracks are related to the internal variables r_{2+} and r_{2-}. The internal variable r_{2-} accounts for compressive damage only, whereas r_{2+} accounts for

both, compressive and tensile, damage. Therefore, for positive transverse normal stresses damage is a function of $d_{2+}\,(r_{2+})$ because both types of cracks ($\alpha = 0°$ and $\alpha = 53°$) are open. Under transverse compressive loads, the damage is only influenced by the inclined cracks, $d_{2-}\,(r_{2-})$.

Kink bands are related to the internal variable r_{1-}. The internal variable r_{1+} accounts for kink bands and fiber tensile fracture. For positive longitudinal normal stresses, the material loses stiffness as a result of both damage modes because the cracks open. Therefore, the damage variable can be expressed as $d_{1+}\,(r_{1+})$.

When a lamina which is fully damaged in tension ($d_{1+} = 1$) is subjected to load reversal and the crack closes, some of the original stiffness is recovered because the tractions can be transmitted through the crack faces. However, the broken fibers lose their alignment. Assuming that the fibers do not carry any load, which can be considered as a limit case, the compressive stiffness can be approximated by the rule of mixtures applied for components in parallel as: $(1 - d_{1-})E_1 = V_m E_m$. The generalization of the above arguments for an intermediate damage state can be expressed as $d_{1-} = A_1^{\pm} d_{1+}$, with:

$$A_1^{\pm} \approx b\frac{V_f E_f}{V_m E_m + V_f E_f} \approx b\frac{E_1 - E_2}{E_1} \tag{27}$$

where E_f and E_m are the fiber and matrix Young modulus, V_f and V_m the corresponding volume fractions, and b is an adjustment parameter between 0 and 1. If $b = 1$ the stiffness recovery is due only by the matrix, and if $b = 0$, the stiffness recovery is total and it is assumed that broken fibers do not lose alignment under compressive loads, and that the initial stiffness is recovered.

Fiber damage ($d_{1\pm}$) is not influenced by matrix cracking ($r_{2\pm}$) as shown in experimental results carried by Carlsson and Pipes [50] and in micromechanical models [51]-[54] of cracked composites. Therefore, the longitudinal stiffness is not function of matrix transverse cracks.

The shear stiffness is reduced as a result of longitudinal and transverse cracks regardless of their orientation. Under these circumstances, the damage variable d_6 is given by:

$$d_6 = 1 - [1 - d_6(r_{2+})](1 - d_{1+}) \tag{28}$$

The damage evolution laws used force strain-softening as soon as one damage activation criterion is satisfied. Softening constitutive equations result in physically inadmissable responses: the damage is localized in a plane and fracture occurs without energy dissipation. The numerical implementation of soften-

ing constitutive equations using the finite element method results in mesh-dependent results because the energy dissipated is a function of the element size.

The solution normally used to ensure the correct computation of the energy dissipated regardless of the refinement of the mesh is to adjust the damage evolution laws using a characteristic dimension of the finite element. The definition of the damage evolution laws is therefore related to the computational model, and will be described in the next section.

4 COMPUTATIONAL MODEL

Two different inelastic responses have to be taken into account in the numerical simulation of damage using Continuum Damage Mechanics. While the stress-strain response of a material exhibits a positive-definite tangent stiffness tensor, the damage zone increases along all the directions. This initial stage of damage is commonly referred to as diffuse damage, and the numerical solution is independent of the numerical discretization. For example, matrix cracking in a multidirectional composite is a form of diffuse damage if the kinematics of laminate theory is used.

When the tangent stiffness tensor is not positive definite, damage localizes in a narrow band, and the numerical solution depends upon the numerical discretization: decreasing the element size in the localized zone decreases the computed energy dissipated. Therefore, the structural response is not objective because it does not converge to a unique solution with mesh refinement.

The proposed damage model uses a constitutive model that forces localization as soon as one of the damage activation functions associated with the onset of transverse or longitudinal cracking is satisfied, i.e., when $F_N = 0$. In order to guarantee that the numerical solution is independent of the discretization a characteristic element length is used in the constitutive model using a procedure based on the crack band model proposed by Bažant [26].

4.1 Damage laws in softening regime: crack band model

Bažant's crack band model [26] assures the objective response of the global finite element model by regularizing the computed dissipated energy using a characteristic dimension of the finite element and the fracture toughness:

$$g_M = \frac{G_M}{l^*},\ M = 1+, 1-, 2+, 2-, 6 \tag{29}$$

where G_M is the fracture toughness, g_M is the energy dissipated per unit volume, and l^* is the characteristic length of the finite element. For square elements, with an aspect ratio approximately equal to one, the characteristic element length can be approximated by the following expression [26]:

$$l^* = \frac{\sqrt{A_{IP}}}{\cos(\gamma)} \tag{30}$$

where $|\gamma| \leq 45^o$ is the angle of the mesh lines with the crack direction and A_{IP} is the area associated at each integration point. For an unknown direction of crack propagation, the average of this expression can be used, $\bar{l}^* = \frac{\pi}{4}\int_0^{\frac{\pi}{4}} l^* d\gamma = 1.12\sqrt{A_{IP}}$.

When the crack propagation path can be estimated in advance, it is recommended to align the mesh with the direction of crack propagation because cracks tend to evolve along the mesh lines. If the crack propagation is aligned with the mesh lines, the characteristic length must be the square root of the area corresponding to an element integration point, i.e., $\gamma = 0$.

For triangular elements, the typical characteristic length is determined by the expression:

$$l^* = 2\sqrt{\frac{A_{IP}}{\sqrt{3}}} \tag{31}$$

A more accurate measure of the characteristic element length would be obtained using the element projections for both possible crack directions, transverse and longitudinal.

The crack band model assumes that the failure process zone can be represented by a damaged finite element zone of one element width. This approximated method for achieving the objectivity of the global response is appropriate for the treatment of large structures under complex damage mechanisms, such as the ones occurring in advanced composites.

The exponential damage evolution laws proposed here are expressed in the following general form:

$$d_M = 1 - \frac{1}{f_N(r_N)} \exp\left\{A_M\left[1 - f_N(r_N)\right]\right\} f(r_K) \tag{32}$$

where the function $f_N(r_N)$ is selected to force the softening of the constitutive relation. $f(r_K)$ is the coupling factor between damage laws and elastic threshold domains.

The damage evolution laws for each damage variable are:

$$\begin{aligned} d_{1+} &= 1 - \tfrac{1}{r_{1+}} \exp[A_{1+}(1 - r_{1+})] \\ d_{1-} &= 1 - \tfrac{1}{r_{1-}} \exp[A_{1-}(1 - r_{1-})] f(A_1^{\pm}, r_{1+}) \\ d_{2+} &= 1 - \tfrac{1}{f_{2+}(r_{2+})} \exp[A_{2+}(1 - f_{2+}(r_{2+}))] \\ d_{2-} &= 1 - \tfrac{1}{r_{2-}} \exp[A_{2-}(1 - r_{2-})] \\ d_6(r_{2+}) &= 1 - \tfrac{1}{r_{2+}} \exp[A_6(1 - r_{2+})] \end{aligned} \tag{33}$$

where $f_{2+}(r_{2+})$ is a function of the same order as the damage onset function in order to force softening:

$$f_{2+}(r_{2+}) = \frac{1}{2g}\left(g - 1 + \sqrt{(1-g)^2 + 4gr_{2+}^2}\right) \tag{34}$$

The coupling factor $A_1^{\pm}$ is used for the interaction of elastic domains in the longitudinal (fiber) direction, and it is defined from equation $d_{1-} = A_1^{\pm} d_{1+}$ and (33) for $r_{1-} = 1$ as:

$$f\left(A_1^{\pm}, r_{1+}\right) = 1 - A_1^{\pm} + A_1^{\pm} \frac{1}{r_{1+}} \exp\left[A_{1+}\left(1 - r_{1+}\right)\right] \tag{35}$$

where $A_1^{\pm}$ is a material parameter defined in equation (27).

The energy dissipated per unit volume for uniaxial stress conditions is obtained by integrating the rate of dissipation, equation (18):

$$g_M = \int_0^{\infty} Y_M \dot{d}_M dt = \int_1^{\infty} \frac{\partial G}{\partial d_M} \frac{\partial d_M}{\partial r_M} dr_M, \;\; M = 1+, 1-, 2+, 2-, 6 \tag{36}$$

Applying the crack band model, equation (29):

$$\int_1^{\infty} \frac{\partial G}{\partial d_M} \frac{\partial d_M}{\partial r_M} dr_M = \frac{G_M}{l^*}, \;\; M = 1+, 1-, 2+, 2-, 6 \tag{37}$$

Using equations (29) and (36) and substituting in (37), it is possible to calculate the damage law parameters A_M that assure that the dissipated energy computed by the numerical model is independent of mesh refinement. It is possible to obtain analytical closed form solutions for two of the equations (37):

$$A_{1+} = \frac{2l^* X_T^2}{2E_1 G_{1+} - l^* X_T^2} \tag{38}$$

$$A_6 = \frac{2l^* S_L^2}{2G_{12} G_6 - l^* S_L^2} \tag{39}$$

The remaining parameters, $A_{2\pm}$ and A_{1-}, are calculated numerically using the algorithm presented in Appendixes A and B. The adjusting parameters complete the definition of the constitutive model.

The material response under load reversal cycles in the transverse and longitudinal direction resulting from the proposed constitutive model are illustrated in Figures 9 and 10 respectively.

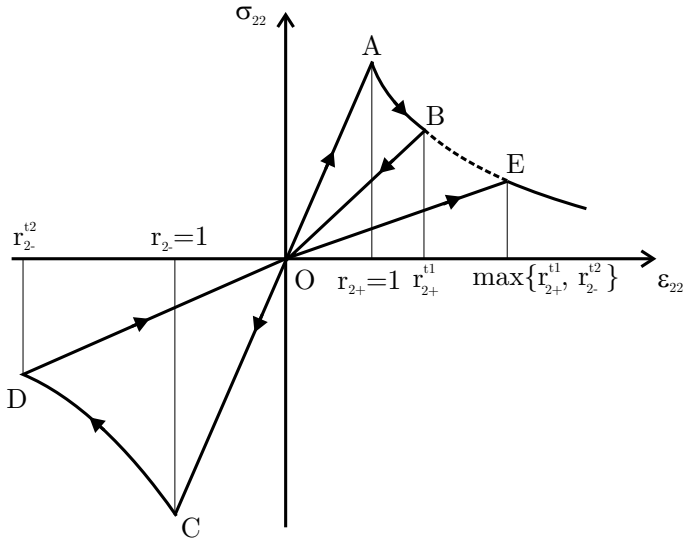

Fig. 9. Transverse load cycle: O-A-B-O-C-D-O-E.

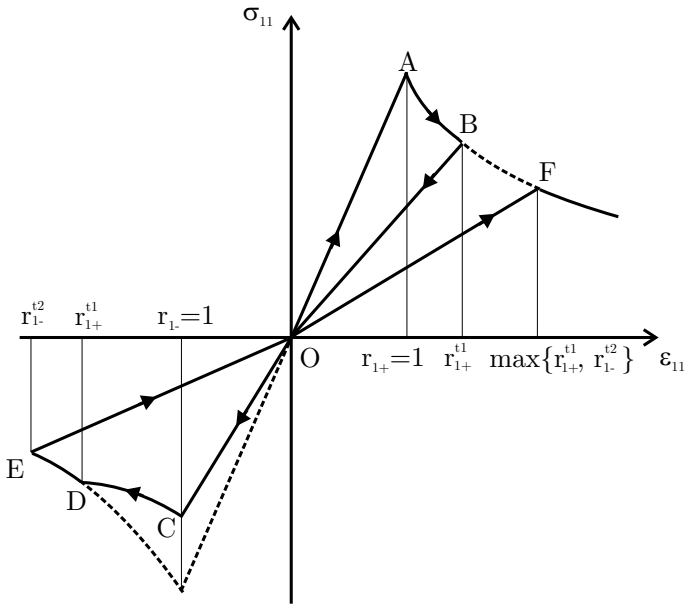

Fig. 10. Longitudinal load cycle: O-A-B-O-C-D-E-O-F.

In the transverse load cycle shown in Figure 9, it can be seen that damage created under tensile stresses (O-A-B-O) does not influence the compressive behavior (O-C), the size of the elastic domain ($r_{2-} = 1$), or the damage variable ($d_{2-} = 0$). On the other hand, damage created under compressive loading (C-D-O) increases the elastic domain in tension (O-E) and affects the damage variable d_{2+}.

In the longitudinal load cycle shown in Figure 10, it can be seen that damage created under tensile loads (O-A-B-O) influences the compressive behavior under load reversal (O-C), corresponding to a decrease of stiffness due the misalignment of the fibers ($d_{1-} = A_1^{\pm} d_{1+}$). However, the elastic domain size remains unchanged ($r_{1-} = 1$).

For damage created under compressive stresses, two regions can be distinguished. For $r_{1-} < r_{1+}$ (C-D), the tensile elastic domain threshold does not change. For $r_{1-} \geq r_{1+}$ (D-E), both elastic domains thresholds increase to reflect the fracture of fibers in compression.

4.1.1 Critical finite element size

The constitutive model must not lead to a local snap-back in the stress-strain relation. In other words, the elastic energy of an element at the onset of localization, which is $X_M^2 \left(l^*\right)^2 t / \left(2E_M\right)$ with $M = 1\pm, 2\pm, 6$, must be lower than or equal to the fracture energy, $G_M l^* t$.

Therefore, the maximum size for the finite element for each damage law M is:

$$l^* \leq \frac{2E_M G_M}{X_M^2}, M = 1\pm, 2\pm, 6 \tag{40}$$

where E_M, G_M and X_M are the Young modulus, fracture energies and strengths, respectively.

If a finite element model consist of elements larger that the maximum size prescribed by equation (40), there is an alternative to further refining the mesh. The snap-back in the constitutive model can be avoided by reducing the corresponding strength [26] while taking the parameter A_M to infinity:

$$X_M = \sqrt{\frac{2E_M G_M}{l^*}} \tag{41}$$

Under these circumstances, the damage variables take two possible values: $d_M = 0$ if $r_N = 1$ or $d_M = 1$ if $r_N > 1$. It is clear that the modification of the strengths, although assuring the correct calculation of the energy dissipated, should not be performed in the elements representing the region where crack initiation, which is controlled by the stress tensor, takes place. In the regions of stress concentrations, where crack initiation is likely to take place, the mesh should be sufficiently refined to avoid any adjustment of the material properties.

4.1.2 Fracture toughness

Each damage evolution function includes one adjusting parameter, $A_M, M = 1\pm, 2\pm, 6$, that needs to be calculated using the corresponding component of the fracture toughness, G_M, representing the energy dissipated by inelastic processes in the fracture process zone.

G_{2+} and G_6 correspond to the fracture toughness of a transverse crack in mode I and II, respectively. The mode I component of the fracture toughness, G_{2+}, can be measured using the Double Cantilever Beam (DCB) test (ASTM-D5528). The mode II component of the fracture toughness, G_6, can be measured using the Four-Point End Notched Flexure (4-ENF) test specimen [28].

G_{1+} corresponds to the mode I component of the fracture toughness for a longitudinal crack. There is no standard test method to measure this property. The suggested test method to measure G_{1+} is the Compact Tension (CT) test specimen proposed by Pinho et al. [28]

The measurement of the energy dissipated that is associated with longitudinal compressive loading is far more complex because several complex dissipative phenomena are involved, such as crack growth, crushing and friction. These events occur sequentially throughout the fracture process and transverse inclined cracks and longitudinal kink bands are the result of the combination of these dissipative mechanisms.

Bažant et al. [55] proposed the following expression to evaluate the energy dissipated in a kink band, G_{1-}:

$$G_{1-} = \frac{w}{s} G_6 \tag{42}$$

where w is the kink band thickness and s is the distance between two matrix cracks. This approximation requires a good knowledge of the kink band geometry in advance, which is a function of the external loads, the geometry of structure and the thickness confinement [56]. This approximation does not take into account other dissipative mechanisms in the material such as sliding of the crack faces. An alternative procedure to measure G_{1-} is to use the compact compression (CC) specimen that triggers kink bands in laminated composites, as proposed by Pinho [28].

The fracture toughness for transverse compression loading, G_{2-} can be calculated approximately using the mode II component of the fracture toughness, the fracture angle α_0 and a term accounting for friction between the crack faces:

$$G_{2-} = \frac{G_6}{\cos\alpha_0} + at\mu Y_C \cos\alpha_0 \approx \frac{G_6}{\cos\alpha_0} + at\eta^T Y_C \cos\alpha_0 \tag{43}$$

where $\alpha_0 \approx 53 \pm 3°$, t is the lamina thickness, and a is an adjustment parameter between 0 (in an unidirectional laminate) and 1 (in a strongly confined lamina).

4.1.3 Viscous regularization

Strain-softening constitutive models cause convergence difficulties when using global solution methods, especially for damage in the longitudinal (fiber) direction. In order to improve the convergence of the numerical algorithm, an artificial Duvaut-Lions viscosity model [57] is implemented. The time derivatives of the internal variables associated with longitudinal failure can be defined as:

$$\dot{r}_{1+} = \frac{\left\langle \max\left\{\phi^s_{1+}, \phi^s_{1-}\right\} - r_{1+}\right\rangle}{\eta} \text{ and } \dot{r}_{1-} = \frac{\left\langle \phi^s_{1-} - r_{1-}\right\rangle}{\eta} \tag{44}$$

where η is the viscous parameter. When η tends to zero and $\langle \max\left\{\phi^s_{1+}, \phi^s_{1-}\right\} - r_{1+}\rangle > 0$, the mathematical definition of a derivative is obtained and the functions (44) tend to the damage thresholds evolution functions defined by equations (25).

A numerical algorithm needs to be implemented for the time integration of the internal variables. Using a backward-Euler scheme, the internal variables can be updated as:

$$\begin{aligned} r^{n+1}_{1-} &= \max\left\{ r^n_{1-}, \frac{\eta}{\eta + \Delta t} r^n_{1-} + \frac{\Delta t}{\eta + \Delta t}\phi^{n+1}_{1-} \right\} \\ r^{n+1}_{1+} &= \max\left\{ r^n_{1+}, r^{n+1}_{1-}, \frac{\eta}{\eta + \Delta t} r^n_{1+} + \frac{\Delta t}{\eta + \Delta t}\phi^{n+1}_{1+} \right\} \end{aligned} \tag{45}$$

Although some materials exhibit time-dependent response, this regularization is implemented with the objective of improving the numerical convergence of the model.

Two undesirable consequences can occur when increasing the viscous parameter. The first one is that the tangent relation becomes positive definite at first stage of damage therefore localization is not ensured at damage onset. Secondly, the energy dissipated at a material integration point undergoing damage evolution increases with the viscous parameter.

4.2 Material tangent constitutive tensor and algorithm

The fast convergence rate of the solution algorithm for the non-linear problem requires the correct computation of the material tangent constitutive tensor, $\mathbf{C}_{\mathrm{T}}$:

$$\dot{\sigma} = \mathbf{C}_{\mathrm{T}} : \dot{\varepsilon} \tag{46}$$

where:

$$\mathbf{C}_{\mathrm{T}} = \mathbf{H}^{-1} : (\mathbf{I} - \mathbf{M}) \tag{47}$$

$\mathbf{H}^{-1}$ is the secant constitutive tensor, $\mathbf{I}$ is the identity tensor and the tensor $\mathbf{M}$ is defined as:

$$\mathbf{M} = \begin{bmatrix} \frac{\sigma_{11}}{(1-d_1)^2 E_1}\frac{\partial d_1}{\partial \varepsilon_{11}} & \frac{\sigma_{11}}{(1-d_1)^2 E_1}\frac{\partial d_1}{\partial \varepsilon_{22}} & \frac{\sigma_{11}}{(1-d_1)^2 E_1}\frac{\partial d_1}{\partial \varepsilon_{12}} \\ \frac{\sigma_{22}}{(1-d_2)^2 E_2}\frac{\partial d_2}{\partial \varepsilon_{11}} & \frac{\sigma_{22}}{(1-d_2)^2 E_2}\frac{\partial d_2}{\partial \varepsilon_{22}} & \frac{\sigma_{22}}{(1-d_2)^2 E_2}\frac{\partial d_2}{\partial \varepsilon_{12}} \\ \frac{\sigma_{12}}{(1-d_6)^2 G_{12}}\frac{\partial d_6}{\partial \varepsilon_{11}} & \frac{\sigma_{12}}{(1-d_6)^2 G_{12}}\frac{\partial d_6}{\partial \varepsilon_{22}} & \frac{\sigma_{12}}{(1-d_6)^2 G_{12}}\frac{\partial d_6}{\partial \varepsilon_{12}} \end{bmatrix} \tag{48}$$

The scalar components of the tensor $\mathbf{M}$ are presented in Appendix C.

The integration of the constitutive model is performed according to the following algorithm:

1	-	Read the strain tensor at time t	ε^{t}
2	-	Compute the effective stress tensor	$\tilde{\sigma}^{\mathrm{t}} = \mathbf{H}_0^{-1} : \varepsilon^{\mathrm{t}}$
3	-	Compute the loading functions	$\phi_M^{\mathrm{t}}(\tilde{\sigma}^{\mathrm{t}})$
4	-	Compute the threshold values	$r_M^{\mathrm{t}}(r_M^{\mathrm{t\text{-}1}}, \phi_M^{\mathrm{t}})$
5	-	Compute the damage variables	$d_M^{\mathrm{t}}(r_M^{\mathrm{t}})$
6	-	Compute the nominal stress tensor	$\sigma^{\mathrm{t}} = \left(\mathbf{H}^{\mathrm{t}}\right)^{-1} : \varepsilon^{\mathrm{t}}$
7	-	Compute the tangent constitutive tensor	$\mathbf{C}_{\mathrm{T}}^{\mathrm{t}} = \left(\mathbf{H}^{\mathrm{t}}\right)^{-1} : (\mathbf{I} - \mathbf{M}^{\mathrm{t}})$

It should be noted that the numerical calculation of the adjusting parameters A_M is only performed once, and only if the damage variable at the integration point is greater than zero. Also, the verification of the condition $A_M \geq 0$ is performed in the beginning of the analysis, and, if it is not satisfied, the material strengths are reduced according to the equation (41).

5 VALIDATION

The model developed was implemented in ABAQUS non-linear finite element code [58] using a user-subroutine UMAT.

The model is validated by comparing the predicted failure loads of quasi-isotropic laminates containing a central hole and loaded in tension with the corresponding experimental data.

The experimental data used was previously obtained by Tan [59] for the open-hole tension test specimen shown in Figure 11. The material consists of T300/1034-C carbon fiber reinforced epoxy with a nominal ply thickness of 0.1308 mm. The elastic properties and unidirectional strengths are shown in Tables 1 and 2 respectively.

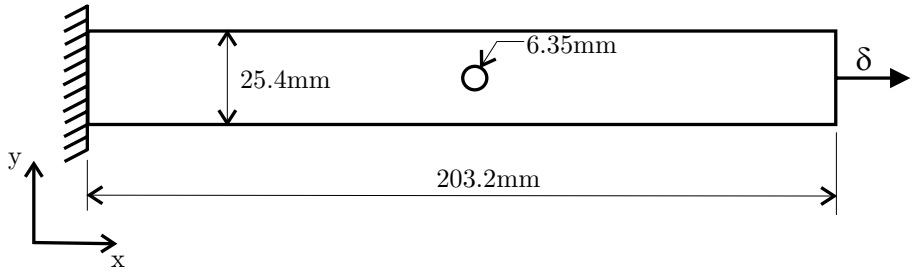

Fig. 11. Configuration of the open-hole tension test specimen.

Table 1
T300/1034-C elastic properties [35],[59].

E_1 (GPa)	E_2 (GPa)	G_{12} (GPa)	ν_{12}
146.8	11.4	6.1	0.30

Table 2
T300/1034-C unidirectional strengths (MPa) [59],[35].

X_T	X_C	Y_T	Y_C	S_L
1730.0	1379.0	66.5	268.2	58.7

The components of the fracture toughness for the different damage models are required for both the determination of the in-situ strengths and of the adjusting parameters $A_M^{\pm}$.

The components of the fracture toughness associated with matrix cracking used in the model were measured by Shahid and Chang [60] for T300/934 carbon-epoxy laminates. The components of the fracture toughness associated with longitudinal tensile and compressive fracture used were obtained by Pinho [28] for a carbon-epoxy composite using the same fiber type (T300/913). The values of fracture toughness used in the model are shown in Table 3.

Table 3
Fracture toughness (N/mm.).

G_{2+}	G_6	G_{2-}	G_{1+}	G_{1-}
0.23	0.46	0.76	89.83	78.27

The damage activation functions are established in terms of the in-situ strengths. The in-situ strengths are calculated from the closed-form equations proposed in [36], using a shear response factor $\beta = 3.2 \times 10^{-8}$ mm^6/N^3. The resulting in-situ strengths are shown in Table 4.

Table 4
In-situ strengths (MPa).

	Embedded ply	Outer ply	Thick ply
Y_T	158.8	101.2	105.4
S_L	109.5	89.8	73.4

The coefficients of thermal expansion of the material used are $\alpha_{11} = -1.0 \times 10^{-6}/°\text{C}$ and $\alpha_{22} = 26.0 \times 10^{-6}/°\text{C}$, and the temperature change is $\Delta T = -152°\text{C}$ [61]. The effects of moisture absorption are neglected in the model.

The lay-ups tested in specimens with the geometry shown in Figure 11 are $[0°/[\pm 45°]_3/90°_3]_s$,$[0°/[\pm 45°]_2/90°_5]_s$ and $[0°/\pm 45°/90°_7]_s$.

The finite element model created use 4-node shell elements. Based on the properties reported in Tables 1-4, the maximum element size that avoids lowering the strength is 0.508 mm. The mesh in the vicinity of the hole, corresponding to the region where damage occurs, consist of elements with sizes ranging from 0.127 mm. (hole edge) to 0.635 mm. (specimen edge).

It is worth noting that shell elements based on lamination theory assume a linear strain field along laminate thickness expressed by two tensors: mid plane strains (ε^0) and curvatures (κ). This simplified kinematic description may not be able to detect the localization of strains in a ply constrained by sub-laminates. In other words, damage mechanisms, such as matrix transverse cracking in just one ply of a multidirectional laminate, correspond to

distributed or diffuse damage if lamination theory is employed. Localization of damage occurs when the different damage mechanisms occur in all plies of the laminate.

Before the localization of damage in the laminate, the ply constitutive models that can be used are based on strain softening, such as in the model proposed here, or on elastic analysis of cracked plies. The latter solution is normally only obtainable for a periodic distribution of transverse matrix cracks in central 90° plies of rectangular laminates under constant stresses [53],[54].

Figure 12 shows the load-displacement relation of the three specimens simulated.

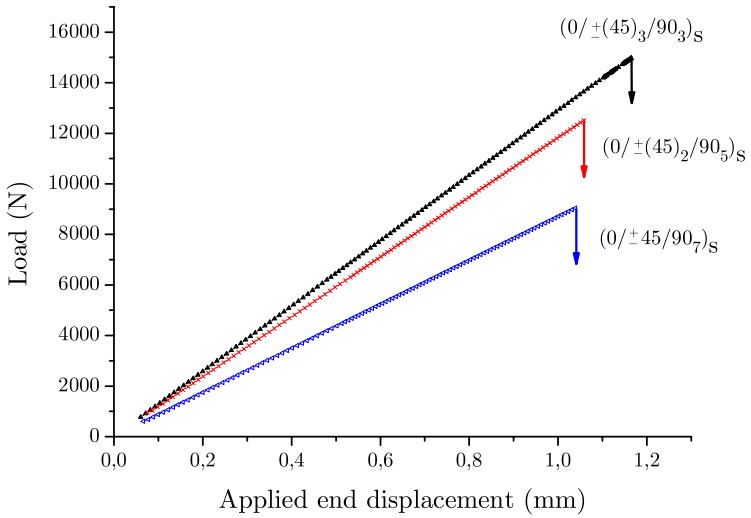

Fig. 12. Predicted load-displacement relations.

Table 5 presents the predicted and experimental failure stresses, σ^N, defined using the failure load P^{u}, and the specimen width and thickness, w and t respectively, as $\sigma^N = \frac{P^{\mathrm{u}}}{wt} = 9.71P^{\mathrm{u}}$.

Table 5
Predicted and measured failure stress, σ^N (MPa).

Lay-up	Experimental [59]	Predicted	Error (%)
$[0°/[\pm45°]_3/90°_3]_s$	235.8	225.5	-4.4
$[0°/[\pm45°]_2/90°_5]_s$	185.8	192.4	3.7
$[0°/\pm45°/90°_7]_s$	160.0	139.3	-12.9

The predicted failure loads are in excellent agreement with the experimental failure loads measured by Tan [59].

6 CONCLUSIONS

A new constitutive model for the prediction of damage onset, growth and ultimate failure of composite structure under plane stress was proposed. The onset of the different intralaminar damage mechanisms is predicted using a simplification of the LaRC04 failure criteria.

The constitutive model proposed is based on four ply fracture planes and accounts for the unilaterality of damage by its ability to represent complex load histories, including tension-compression load reversals.

The constitutive law was implemented in a computational model that ensures that the computed dissipated energy is independent of the discretization. Therefore, the numerical solution is objective with respect to mesh refinement.

The computational model developed was used in the simulation of open-hole test specimens loaded in tension using different lay-ups. An excellent agreement between the predicted and measured failure stresses was obtained.

Acknowledgements

The research stays of the first author at the University of Porto, Portugal, were funded by the University of Girona (BE-UdG-2004) and by the Spanish government under "Acciones Integradas Hispano-Portuguesas" (HIP2004-0031). The first and third authors also acknowledges the funds of the Spanish government through DGICYT under the contract MAT 2003-09768-C03-01.

The financial support of the Portuguese Foundation for Science and Technology (FCT) under the project PDCTE/50354/EME/2003 is acknowledged by the second author.

References

[1] *MIL-HDBK-17-3F, Military Handbook, Polymer Matrix Composites.* U.S. Department of Defense (2002).

[2] Soden P. D., Hinton M. J., Kaddour A. S., *A comparison of the predictive capabilities of current failure theories for composite laminates*, Composites Science and Technology, Vol. 58, No. 7, (1998) pp. 1225-1254.

[3] Dávila C. G., Camanho P. P., Rose C. A., *Failure criteria for FRP laminates*, Journal of Composite Materials, **39** (2005) pp. 323-345.

[4] Pinho S. T., Dávila C. G., Camanho P. P., Ianucci L., Robinson P., *Failure models and criteria for FRP under in-plane or three-dimensional stress states including shear non-linearity*. NASA/TM-2003-213530 (2004).

[5] Kachanov L. M., *Time of the rupture process under creep conditions*. Isv. Nauk SSSR, Otd. Tehk. Nauk, **8** (1958) pp. 26-31.

[6] Chaboche J-L., *A continuum damage theory with anisotropic and unilateral damage*. La Recherche Aérospatiale **2** (1995) pp. 139-147.

[7] Carol I., Rizzi E., Willam K., *On the formulation of anisotropic elastic degradation. I. Theory based on a pseudo-logarithmic damage tensor rate*. Int. J. Solid Structures **38** (2001) pp. 491-518.

[8] Carol I., Rizzi E., Willam K., *On the formulation of anisotropic elastic degradation. II. Generalized pseudo-Rankine model for tensile damage*. Int. J. Solid Structures **38** (2001) pp. 519-546.

[9] Luccioni B., Oller S., *A directional damage model*. Comput. Methods Appl. Mech. Engrg. **192** (2003) pp. 1119-1145.

[10] Ortiz M., *A constitutive theory for inelastic behaviour of concrete.* Mechanics of Materials **4** (1985) pp. 67-93.

[11] Simo J. C., Ju J. W., *Strain and stress-based continuum damage models-I. Formulation*. Int. J. Solids Structures **23**(23) (1987) pp. 821-840.

[12] Simo J. C., Ju J. W., *Strain and stress-based continuum damage models-II. Computational aspects*. Int. J. Solids Structures **23**(23) (1987) pp. 841-869.

[13] Cauvin A., Testa R. B., *Damage mechanics: basic variables in continuum theories*. Int. J. Solid Structures **36** (1999) pp. 747-761.

[14] Chaboche J-L., Kruch S., Maire J. F., Pottier T., *Towards a micromechanics based inelastic and damage modeling of composites*. Int. J. of plasticity **17** (2001) pp. 411-439.

[15] Fish J., Yu Q., *Two-scale damage modeling of brittle composites*. Comp. Science and Technology **61** (2001) pp. 2215-2222.

[16] Fish J., Yu Q., Shek K., *Computational damage mechanics for composite materials based on mathematical homogenization*. Int. J. Numer. Meth. Engng. **45** (1999) pp. 1657-1679.

[17] Voyiadjis G. Z., Deliktas B., *A coupled anisotropic damage model for the inelastic response of composite materials*. Comput. Methods Appl. Mech. Engrg. **183** (2000) pp. 159-199.

[18] Car E., Zalamea F., Oller S., Miquel J., Oñate E., *Numerical simulation of fiber reinforced composite materials — two procedures*. Int. J. Solid Structures **39** (2002) pp. 1967-1986.

[19] Oller S., Miquel Canet J., Zalamea F., *Composite material behavior using a homogenization double scale method.* Journal of Engineering Mechanics **31**(1) (2005) pp. 65-79.

[20] Ladevèze P., Allix O., Deü J-F., Lévêque D., *A mesomodel for localisation and damage computation in laminates*. Comput. Methods Appl. Mech. Engrg. **183** (2000) pp. 105-122.

[21] Barbero E. J., Lonetti P., *A damage model for composites defined in terms of available data*. J. Mech. Compos. Mater. Struct. **8**(4) (2001) pp. 299-316.

[22] Barbero E. J., Devivo L., *A constitutive model for elastic damage in fiber-reinforced PMC laminae*. J. Damage. Mech. **10**(1) (2001) pp. 73-93.

[23] Matzenmiller A., Lubliner J., Taylor R. L., *A constitutive model for anisotropic damage in fiber-composites.* Mechanics of Materials **20** (1995) pp. 125-152.

[24] Oller S., Botello S., Miquel J., Oñate E., *An anisotropic elastoplastic model based on an isotropic formulation.* Engineering Computations **12** (1995) pp. 245-262.

[25] William K. V., Vaziri R., Poursartip A., *A physically based continuum damage mechanics model for thin laminated composite structures*. Int. J. Solids and Structures **40** (2003) pp. 2267-2300.

[26] Bažant Z. P., Oh B. H., *Crack band theory for fracture of concrete.* Materials and structures **16** (1983) pp. 155-177.

[27] Daniel I. M., Ishai O., *Engineering mechanics of composite materials*. Oxford Univerity Press (1994).

[28] Pinho S. T., *Modelling failure of laminated composites using physically-based failure models*. PhD Thesis, Department of Aeronautics, Imperial College London, U.K. (2005).

[29] Fleck N. A., Liu D., *Microbuckle initiation from a patch of large amplitude fibre waviness in a composite under compression and bending*. European Journal of Mechanics - A/Solids, **20**(1) (2001) pp. 23-37.

[30] Schultheisz C. R., Waas A. M., *Compressive failure of composites, Part 1: Testing and micromechanical theories*. Progress in Aerospace Sciences, **32** (1996) pp. 1-42.

[31] Camanho, P. P., *Application of numerical methods to the strength prediction of mechanically fastened joints in composite laminates*. PhD Thesis, Centre for Composite Materials, Department of Aeronautics, Imperial College London, U.K. (1999).

[32] Argon A. S., *Fracture of Composites, Vol. 1*. Academic Press, New York, (1972).

[33] Sutcliffe M. P. F., Fleck N. A., *Microbuckle propagation in fibre composites*. Acta mater. **45**(3) (1997) pp. 921-932.

[34] Parvizi A., Garrett K., Bailey J., *Constrained cracking in glass fibre-reinforced epoxy cross-ply laminates*. Journal of Material Science, **13** (1978) pp. 195-201.

[35] Chang F. K., Chen M. H., *The in-situ ply shear strength distributions in graphite/epoxy laminated composites*. Journal of Composite Materials. **21** (1987) pp. 708-733.

[36] Camanho P. P., Dávila C. G., Pinho S. T., Iannucci, L., Robinson, P., *Prediction of in-situ strengths and matrix cracking in composites under transverse tension and in-plane shear*. Composites- Part A, in press (2005).

[37] Dvorak G. J., Laws N., *Analysis of progressive matrix cracking in composite laminates II. First ply failure.* Journal of Composite Materials. **21** (1987) pp. 309-329.

[38] Swanson S. R., Messick M. J., Tian Z., *Failure of carbon epoxy lamina under combined stresses*. J. Composite Materials, **21** (1987) pp. 619-630.

[39] Swanson S. R., *A micro-mechanical model for in-situ compression strength of fiber composite laminates*. Transactions of the American Society of Mechanical Engineers. Series H, Journal of Engineering Materials and Technology **114** (1992) pp. 8-12.

[40] Puck A., Schürmann H., *Failure analysis of FRP laminates by means of physically based phenomenological models*. Composites Science and Technology. **58** (1998) pp. 1045-1067.

[41] Camanho P. P., Dávila C. G., *Mixed-mode decohesion finite elements for the simulation of delamination in composite materials*. NASA/TM-2002-211737 (2002).

[42] Turon A., Camanho P. P., Costa J., Dávila C. G., *An interface damage model for the simulation of delamination under variable mode ratio in composite materials*. NASA TM 213277 (2004).

[43] Camanho P. P., Dávila C. G., Ambur D. R., *Numerical simulation of delamination growth in composite materials.* NASA-TP-2001-211041 (2001).

[44] Allix O., Daudeville L., Ladevèze, P., *Delamination and damage mechanics*. Mechanical Engineering Publications, London. (1991) pp. 143-157.

[45] Dudgale D. S., *Yielding of steel sheets containing slits.* Journal of Mechanics and Physics of Solids **8** (1960) pp. 100-104.

[46] Barenblatt G. I., *Mathematical theory of equilibrium cracks in brittle fracture.* Advances in Applied Mechanics **7** (1962).

[47] Malvern L. E., *Introduction to the mechanics of a continuous medium.* Prentice-Hall, Englewood Cliffs (1969).

[48] Chaboche J-L., Maire J. F., *A new micromechanics based CDM model and its application to CMC's.* Aerospace Science and Technology **6** (2002) pp. 131-145.

[49] Carol I., Willam K. *Spurious dissipation/generation in stiffness recovery models for elastic degradation and damage.* Int. J. Solid Structures **33** (1996) pp. 2939-2957.

[50] Carlsson L. A., Pipes R. B., *Experimental characterization of composite materials.* Prentice-Hall (1987).

[51] Dvorak G. J., Laws N., Hejazi M., *Analysis of progressive matrix cracking in composite laminates I. thermoelastic properties of a ply with cracks.* Journal of Composite Materials. **19** (1985) pp. 216-234.

[52] Laws N., Dvorak G. J., Hejazi M., *Stiffness changes in unidirectional composites caused by crack systems.* Mechanics of Materials. **2** (1983).

[53] Nuismer R. J., Tan S. C., *Constitutive relations of a cracked composite lamina.* Journal of Composite Materials. **22** (1988) pp. 306-321.

[54] Tan S. C., Nuismer R. J., *A theory for progressive matrix cracking in composite laminates.* Journal of Composite Materials. **23**(1989) pp. 1029-1047.

[55] Bažant Z. P., Kim J-J. H., Daniel I. M., Becq-Giraudon E., Zi G., *Size effect on compression strength of fiber composites failing by kink band propagation.* International Journal of fracture. **95** (1999) pp. 103-141.

[56] McGee J. D., Nemat-Nasser S., *Dynamic bi-axial testing of woven composites.* Material Science and Engineering **A317** (2001) pp. 135-139.

[57] Duvaut G., Lions J. L., *Les inéquations en mécanique et en physique.* Dunod, Paris (1972).

[58] ABAQUS 6.5 User's Manual, ABAQUS Inc., Pawtucket, RI, U.S.A. (2005).

[59] Tan S. C., *A progressive failure model for composite laminates containing openings.* Journal of Composite Materials. **25** (1991) pp. 556-577.

[60] Shahid I. S., Chang F. K., *An accumulative damage model for tensile and shear failures of laminated composite plates.* Journal of Composite Materials. **29** (1995) pp. 926-981.

[61] Springer G. S., *Environmental effects on composite materials.* Technomic Publishing Company, Inc., Westport, U.S.A. (1981).

Appendix A: Integration Algorithm

In order to calculate the adjusting parameters A_M used in the damage evolution laws, it is necessary to integrate the following equation numerically:

$$g_M = \int_1^{\infty} \left(\frac{1 - \nu_{12}\nu_{21}}{1 - (1 - d_M)\,\nu_{12}\nu_{21}} \right)^2 \frac{\tilde{\sigma}_M^2}{2E_M} \frac{\partial d_M}{\partial r_N} dr_N \tag{A-1}$$

The Simpson method of numerical integration approximates the solution using quadratic polynomials. The general form of the polynomial can be expressed as:

$$g_M \simeq \frac{h}{3} \left(f_M^0 + ... + 4f_M^{odd} + 2f_M^{even} + ... + f_M^n \right) \tag{A-2}$$

where h is the step increment, and $f_M^i = \left(\frac{1-\nu_{12}\nu_{21}}{1-\left(1-d_M^i\right)\nu_{12}\nu_{21}} \right)^2 \frac{\left(\tilde{\sigma}_M^i\right)^2}{2E_M^i} \frac{\partial d_M^i}{\partial r_N^i}$ is defined between $r = 1$ and $r \to \infty$.

Since the damage laws selected tend to zero, it is necessary to define a point to stop the integration. When the stress becomes less than K times the stress at the onset of localization, the remaining energy can be neglected. The increment *(h)* can be selected defining the number of steps *(n)* as:

$$h_i \approx -\frac{1}{nA} \ln \left(\frac{1}{K} \right) \tag{A-3}$$

The algorithm is implemented as:

1- Select the parameters n and K

2- Initialize r=1 , G=0 and CONT=0

3- Compute step size h

4- WHILE CONT<n

DO I=1:3

$$f(I) = \left(\frac{1-\nu_{12}\nu_{21}}{1-(1-d_M)\nu_{12}\nu_{21}}\right)^2 \frac{\tilde{\sigma}_M^2}{2E_M} \frac{\partial d_M}{\partial r_N}$$

r=r+h

END DO

r=r-h

$g = g + \frac{h}{3}\left(f(1) + 4f(2) + f(3)\right)$

CONT=CONT+1

END WHILE

Appendix B: Secant method to determine the parameters A_M

To find the adjustment parameters for the damage law, it is necessary to integrate the stress-strain relation in terms of the unknown parameter A_M. The integration can be done numerically with the algorithm presented in Appendix A. To iterate on the value of A_M, the secant method is used. The problem to be solved can be expressed as:

$$g_M\left(A_M\right) - \frac{G_M}{l^*} = 0 \tag{B-1}$$

To select the two parameters to start the iteration, the following approximation is used:

$$A_M^1 = \frac{2l^* X_M^2}{2E_M G_M - l^* X_M^2} \text{ and } A_M^0 = 0.5A_M^1 \tag{B-2}$$

The function $g_i\left(A_i\right)$ is only defined for positives values of A. Defining the minimization function as:

$$\ln\left(A_M^{j+1}\right) = \ln\left(A_M^j\right) - \left[\ln\left(g_M^j\right) - \ln\left(\frac{G_M}{l^*}\right)\right] \frac{\ln\left(A_M^j\right) - \ln\left(A_M^{j-1}\right)}{\ln\left(g_M^j\right) - \ln\left(g_M^{j-1}\right)} \tag{B-3}$$

the following algorithm is proposed:

1-	Initialize	$A_M^1 = \frac{2l^* X_M^2}{2E_M G_M - l^* X_M^2}$, $A_M^0 = 0.5A_M^1$ and j=1
2-	Integrate numerically	g_M^0 , see Appendix A
	WHILE $\left\lvert g_M\left(A_M\right) - \frac{G_M}{l^*}\right\rvert \leq tol$	
		Integrate numerically g_M^j , see Appendix A
		$A_M^{j+1} = \exp^{\ln\left(A_M^j\right) - \left[\ln\left(g_M^j\right) - \ln\left(\frac{G_M}{l^*}\right)\right] \frac{\ln\left(A_M^j\right) - \ln\left(A_M^{j-1}\right)}{\ln\left(g_M^j\right) - \ln\left(g_M^{j-1}\right)}}$
		$g_M^{j+1} = g_M^j$
		$A_M^j = A_M^{j-1}$
		j=j+1
	END WHILE	

Appendix C: Material tangent stiffness tensor

If artificial viscosity is considered, incremental damage laws have to be implemented:

$$\frac{\partial d_1}{\partial r_1} = \frac{\partial d_1^{n+1}}{\partial r_1^{n+1}} \frac{\partial r_1^{n+1}}{\partial r_1^n} = \frac{\partial d_1^{n+1}}{\partial r_1^{n+1}} \left(\frac{\eta}{\Delta t + \eta} \frac{\partial r_1^n}{\partial r_1^{n-1}} + \frac{\Delta t}{\Delta t + \eta} \right) \tag{C-1}$$

Applying the chain rule, the damage evolution can be written as:

$$\left[\begin{array}{ccc} \frac{\partial d_1}{\partial \varepsilon_{11}} & \frac{\partial d_1}{\partial \varepsilon_{22}} & \frac{\partial d_1}{\partial \varepsilon_{12}} \end{array} \right] = \frac{\partial d_1}{\partial r_1} \left[\begin{array}{ccc} \frac{\partial r_1}{\partial \varepsilon_{11}} & \frac{\partial r_1}{\partial \varepsilon_{22}} & \frac{\partial r_1}{\partial \varepsilon_{12}} \end{array} \right]$$

$$\left[\begin{array}{ccc} \frac{\partial d_2}{\partial \varepsilon_{11}} & \frac{\partial d_2}{\partial \varepsilon_{22}} & \frac{\partial d_2}{\partial \varepsilon_{12}} \end{array} \right] = \frac{\partial d_2}{\partial r_2} \left[\begin{array}{ccc} \frac{\partial r_2}{\partial \varepsilon_{11}} & \frac{\partial r_2}{\partial \varepsilon_{22}} & \frac{\partial r_2}{\partial \varepsilon_{12}} \end{array} \right]$$

$$\left[\begin{array}{ccc} \frac{\partial d_6}{\partial \varepsilon_{11}} & \frac{\partial d_6}{\partial \varepsilon_{22}} & \frac{\partial d_6}{\partial \varepsilon_{12}} \end{array} \right] = \left(1 - d_6\left(r_1\right)\right) \frac{\partial d_6(r_2)}{\partial r_2} \left[\begin{array}{ccc} \frac{\partial r_2}{\partial \varepsilon_{11}} & \frac{\partial r_2}{\partial \varepsilon_{22}} & \frac{\partial r_2}{\partial \varepsilon_{12}} \end{array} \right] +$$

$$+ \left(1 - d_6\left(r_2\right)\right) \frac{\partial d_6(r_1)}{\partial r_1} \left[\begin{array}{ccc} \frac{\partial r_1}{\partial \varepsilon_{11}} & \frac{\partial r_1}{\partial \varepsilon_{22}} & \frac{\partial r_1}{\partial \varepsilon_{12}} \end{array} \right]$$

Derivation of softening damage laws:

$$\frac{\partial d_N}{\partial r_M} = \frac{1 + r_M A_N}{r_M^2} \exp\left[A_N\left(1 - r_M\right)\right]$$

$$\frac{\partial d_{1-}}{\partial r_{1-}} = \begin{cases} \frac{1 + r_{1-} A_{1-}}{r_{1-}^2} \exp\left[A_{1-}\left(1 - r_{1-}\right)\right] f\left(A_1^{\pm}, r_{1+}\right) & \text{if } r_{1+} > r_{1-} \\ \frac{1 + r_{1-} A_{1-}}{r_{1-}^2} \exp\left[A_{1-}\left(1 - r_{1-}\right)\right] K_{1-} & \text{if } r_{1+} = r_{1-} \end{cases}$$

$$\frac{\partial d_{2+}}{\partial r_{2+}} = 4 \frac{g r_{2+} \exp(A_{2+}(1 - K_{2+}))(g(2 + A_{2+}) - A_{2+}(1 - K_{2+}))}{K_{2+}(g - 1 + K_{2+})}$$

$$\frac{\partial d_6\left(r_1\right)}{\partial r_1} = \frac{1 + r_{1+} A_{1+}}{r_{1+}^2} \exp\left(A_{1+}\left(1 - r_{1+}\right)\right)$$

Where:

$$K_{1-} = f\left(A_1^{\pm}, r_{1+}\right)\left(1 + r_{1-} A_{1-}\right) + \frac{A_1^{\pm}}{r_{1-}}\left(1 + r_{1-} A_{1+}\right) \exp\left[A_{1+}\left(1 - r_{1-}\right)\right]$$

$$f\left(A_1^{\pm}, r_{1+}\right) = 1 - A_1^{\pm} + A_1^{\pm} \frac{1}{r_{1+}} \exp\left[A_{1+}\left(1 - r_{1+}\right)\right]$$

and $K_{2+} = \sqrt{(1 - g)^2 + 4 g r_{2+}^2}$

Evolution of damage thresholds respect the strains:

$$\left[\begin{array}{ccc} \frac{\partial r_{1+}}{\partial \varepsilon_{11}} & \frac{\partial r_{1+}}{\partial \varepsilon_{22}} & \frac{\partial r_{1+}}{\partial \varepsilon_{12}} \end{array}\right] = \frac{E_1}{X_T}\left[\begin{array}{ccc} 1 & 0 & 0 \end{array}\right]$$

$$\left[\begin{array}{ccc} \frac{\partial r_{1-}}{\partial \varepsilon_{11}} & \frac{\partial r_{1-}}{\partial \varepsilon_{22}} & \frac{\partial r_{1-}}{\partial \varepsilon_{12}} \end{array}\right] = \begin{cases} \frac{1}{S_L}\left[\begin{array}{ccc} 0 & \eta^L & \text{sign}\left(\tilde{\sigma}_{12}^m\right) \end{array}\right][\mathbf{R}]\,[\mathbf{C}^0] & \text{if } \frac{\left\langle\left|\tilde{\sigma}_{12}^m\right|+\eta^L\tilde{\sigma}_{22}^m\right\rangle}{S_L} < \frac{-E_1}{Y_C}\varepsilon_{11} \\ \frac{E_1}{Y_C}\left[\begin{array}{ccc} 1 & 0 & 0 \end{array}\right] & \text{if } \frac{\left\langle\left|\tilde{\sigma}_{12}^m\right|+\eta^L\tilde{\sigma}_{22}^m\right\rangle}{S_L} > \frac{-E_1}{Y_C}\varepsilon_{11} \end{cases}$$

$$\left[\begin{array}{ccc} \frac{\partial r_{2+}}{\partial \varepsilon_{11}} & \frac{\partial r_{2+}}{\partial \varepsilon_{22}} & \frac{\partial r_{2+}}{\partial \varepsilon_{12}} \end{array}\right] = \begin{cases} \frac{1}{r_{2+}}\left[\begin{array}{ccc} 0 & \frac{1-g}{2Y_T}+\frac{g\tilde{\sigma}_{22}}{Y_T^2} & \frac{\tilde{\sigma}_{12}}{S_L^2} \end{array}\right][\mathbf{C}^0] \text{ if } \tilde{\sigma}_{22} > 0 \\ \frac{1}{S_L}\left[\begin{array}{ccc} 0 & \eta^L & \text{sign}\left(\tilde{\sigma}_{12}\right) \end{array}\right][\mathbf{C}^0] \quad \text{if } \tilde{\sigma}_{22} < 0 \end{cases}$$

$$\left[\begin{array}{ccc} \frac{\partial r_{2-}}{\partial \varepsilon_{11}} & \frac{\partial r_{2-}}{\partial \varepsilon_{22}} & \frac{\partial r_{2-}}{\partial \varepsilon_{12}} \end{array}\right] = \begin{cases} \frac{1}{r_{2-}}\left(\frac{\tilde{\sigma}_{\text{eff}}^T}{S_T^2}\frac{\partial \tilde{\sigma}_{\text{eff}}^T}{\partial \varepsilon}+\frac{\tilde{\sigma}_{\text{eff}}^L}{S_L^2}\frac{\partial \tilde{\sigma}_{\text{eff}}^L}{\partial \varepsilon}\right) \text{ if } \quad \left(\frac{\tilde{\sigma}_{\text{eff}}^T}{S_T}\right)^2+\left(\frac{\tilde{\sigma}_{\text{eff}}^L}{S_L}\right)^2 < \varepsilon_{22} \\ \frac{E_2}{Y_T}\left[\begin{array}{ccc} 0 & 1 & 0 \end{array}\right] \qquad \text{if } \left(\frac{\tilde{\sigma}_{\text{eff}}^T}{S_T}\right)^2+\left(\frac{\tilde{\sigma}_{\text{eff}}^L}{S_L}\right)^2 > \frac{E_{22}}{Y^T}\varepsilon_{22} \end{cases}$$

Where:

$$[\mathbf{R}] = \begin{bmatrix} \cos^2\varphi^C & \sin^2\varphi^C & 2\cos\varphi^C\sin\varphi^C\text{sign}\left(\tilde{\sigma}_{12}\right) \\ \sin^2\varphi^C & \cos^2\varphi^C & -2\cos\varphi^C\sin\varphi^C\text{sign}\left(\tilde{\sigma}_{12}\right) \\ -\cos\varphi^C\sin\varphi^C & \cos\varphi^C\sin\varphi^C & \left(\cos^2\varphi^C-\sin^2\varphi^C\right)\text{sign}\left(\tilde{\sigma}_{12}\right) \end{bmatrix}$$

$$\frac{\partial \tilde{\sigma}_{\text{eff}}^T}{\partial \varepsilon} = \left[\begin{array}{ccc} 0 & -\cos\alpha_0\left(\sin\alpha_0-\frac{\eta^T\cos\alpha_0}{K}\right)+\frac{\eta^T}{K^3}\left(\frac{\tilde{\sigma}_{12}}{\tan\alpha_0\ \tilde{\sigma}_{22}}\right)^2 & -\frac{\eta^T\tilde{\sigma}_{12}}{\tilde{\sigma}_{22}K^3\tan^2\alpha_0} \end{array}\right][\mathbf{C}^0]$$

$$\frac{\partial \tilde{\sigma}_{\text{eff}}^L}{\partial \varepsilon} = \left[\begin{array}{ccc} 0 & \frac{\eta^L\cos^2\alpha_0}{K^3\sin^3\alpha_0}\frac{|\tilde{\sigma}_{12}|^3}{\tilde{\sigma}_{22}^3} & \frac{\eta^L\cos\alpha_0}{K\tan\alpha_0}+\text{sign}\left(\tilde{\sigma}_{12}\right)\cos\alpha_0\left(1-\frac{\eta^L\cos\alpha_0}{K^3\sin^3\alpha_0}\frac{\tilde{\sigma}_{12}^2}{\tilde{\sigma}_{22}^2}\right) \end{array}\right][\mathbf{C}^0]$$

and $K = \sqrt{1+\frac{\tilde{\sigma}_{12}^2}{\tilde{\sigma}_{22}^2\sin^2\alpha_0}}$

REPORT DOCUMENTATION PAGE

Form Approved
OMB No. 0704-0188

1. REPORT DATE *(DD-MM-YYYY)*	2. REPORT TYPE	3. DATES COVERED *(From - To)*
15-03-2006	Technical Memorandum	

4. TITLE AND SUBTITLE

A Thermodynamically Consistent Damage Model for Advanced Composites

5a. CONTRACT NUMBER

5b. GRANT NUMBER

5c. PROGRAM ELEMENT NUMBER

6. AUTHOR(S)

Pere Maimí; Pedro P. Camanho; Joan-Andreu Mayugo; Carlos G. Dávila

5d. PROJECT NUMBER

5e. TASK NUMBER

5f. WORK UNIT NUMBER

7. PERFORMING ORGANIZATION NAME(S) AND ADDRESS(ES)

NASA Langley Research Center
Hampton, VA 23681-2199

8. PERFORMING ORGANIZATION REPORT NUMBER

L-19239

9. SPONSORING/MONITORING AGENCY NAME(S) AND ADDRESS(ES)

National Aeronautics and Space Administration
Washington, DC 20546-0001

10. SPONSORING/MONITOR'S ACRONYM(S)

NASA

11. SPONSORING/MONITORING REPORT NUMBER

NASA/TM-2006-214282

12. DISTRIBUTION/AVAILABILITY STATEMENT

Unclassified - Unlimited
Subject Category 39
Availability: NASA CASI (301) 621-0390

13. SUPPLEMENTARY NOTES

Maimí and Mayugo: University of Girona; Camanho: University of Porto; Dávila: Langley Research Center

14. ABSTRACT

A continuum damage model for the prediction of damage onset and structural collapse of structures manufactured in fiber-reinforced plastic laminates is proposed. The principal damage mechanisms occurring in the longitudinal and transverse directions of a ply are represented by a damage tensor that is fixed in space. Crack closure under load reversal effects are taken into account using damage variables established as a function of the sign of the components of the stress tensor. Damage activation functions based on the LaRC04 failure criteria are used to predict the different damage mechanisms occurring at the ply level. The constitutive damage model is implemented in a finite element code. The objectivity of the numerical model is assured by regularizing the dissipated energy at a material point using Bazant's Crack Band Model. To verify the accuracy of the approach, analyses of coupon specimens were performed, and the numerical predictions were compared with experimental data.

15. SUBJECT TERMS

Fracture Mechanics; Continuum Damage Mechanics; Failure Criteria; Composite Materials.

16. SECURITY CLASSIFICATION OF:			17. LIMITATION OF ABSTRACT	18. NUMBER OF PAGES	19a. NAME OF RESPONSIBLE PERSON
a. REPORT	b. ABSTRACT	c. THIS PAGE			STI Help Desk (email: help@sti.nasa.gov)
U	U	U	UU	47	19b. TELEPHONE NUMBER *(Include area code)* (301) 621-0390